CDF/ANAL/EXOTIC/CDFR/9268
Draft 2.0
April 6, 2008

Search for Technicolor Particle in Association with $W^{\pm}$ Boson at CDF with $\int \mathcal{L}dt$ = 1.9 fb^{-1}

Shinhong Kim[1], Tatsuya Masubuchi[1], Yoshikazu Nagai[1],Weiming Yao[2]

[1]*University of Tsukuba*
[2]*LBNL*

Abstract

We present a search for Technicolor particles decaying into $b\bar{b}$, $b\bar{c}$ or $b\bar{u}$ and produced in association with $W^{\pm}$ bosons in $p\bar{p}$ collisions at $\sqrt{s} = 1.96$ TeV. This search uses data through period 12, corresponding to an integrated luminosity of 1.9 fb^{-1}. We select at least one tagged $W^{\pm}+2$ jets events that fall into one of the three categories: Events with two tight SECVTX tags, events with one tight SECVTX tag plus one jet probability tag or events with one tight SECVTX tag. Furthermore, neural network b-tagging algorithm is applied to the one tight SECVTX tag events to improve the background separation. The number of tagged events and the invariant mass distributions of $W^{\pm} + 2$ jets and dijets are consistent with the Standard Model expectations. We set a 95% confidence level upper limit on the production cross section times branching ratio as a function of the Technicolor particle masses.

1 Introduction

For several decades, the Standard Model has been remarkably successful in explaining and predicting experimental data. However, the mechanism of electroweak symmetry breaking is still not known. The two most popular mechanisms to induce spontaneous symmetry breaking of a gauge theory, resulting in the gauge bosons and fermions acquiring masses, are the Higgs mechanism and the dynamics of a new interaction such as Technicolor. Both mechanisms predict the existence of a new particle X with unknown mass which could be produced at the Tevatron through $p\bar{p} \rightarrow W^{\pm}X$. In this note, we especially present a search for Technirho ($\rho_T^{\pm/0}$) and Technipion ($\pi_T^{0/\mp}$) through $p\bar{p} \rightarrow \rho_T \rightarrow W^{\pm}\pi_T$ using the SECVTX b-tagger, jet probability b-tagger and LBL NN b-tagger[5, 6]. Technicolor production cross section in p$\bar{\text{p}}$ collisions at $\sqrt{s} = 1.96$ TeV has the order of a few pb depending on the parameters and $m(\rho_T), m(\pi_T)$ mass [1]. Figure 1 shows the Feynman diagrams of Technicolor production searched in this note.

The search signature considered here is $\rho_T^{\pm/0} \rightarrow W^{\pm}\pi_T^{0/\mp}$ with $W^{\pm} \rightarrow e\nu$ or $\mu\nu$, and $\pi_T^0 \rightarrow b\bar{b}$, $\pi_T^+ \rightarrow \bar{b}c, \bar{b}u$ or $\pi_T^- \rightarrow b\bar{c}, b\bar{u}$, giving final states with one high p_T lepton, large missing E_T ($\not\!\!E_T$) and one or two b jets. We focus our attention on the $W^{\pm}+2$ jets signature since it contains most of the signal, while b-tagged $W^{\pm}+ \geq 3$ jets events are dominated by $t\bar{t}$ decays.

The previous Technicolor search[2] was performed with data corresponding to a integrated luminosity of 955 pb^{-1} and excluded the $m(\pi_T)$ mass region at 95 $\sim$ 98 GeV at $m(\rho_T) =$ 190 GeV.

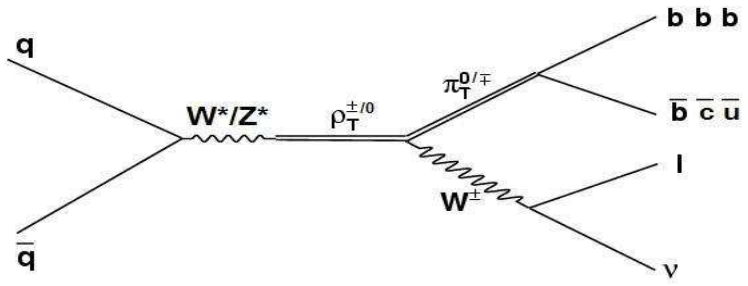

Figure 1: The Feynman diagram of $p\bar{p} \to W^*/Z^* \to \rho_T^{\pm/0} \to W^{\pm}\pi_T^{0/\mp} \to l\nu b\bar{b}/b\bar{c}, b\bar{u}$

2 Data sample and Luminosity Calculation

The data used this analysis are the high p_T central electron **bhel0d**, **bhel0h**, **bhel0i** or **bhel0j** and the high p_T central muon **bhmu0d**, **bhmu0h**, **bhmu0i** or **bhmu0j**, which are collected through March 2007. We select the events from these datasets that pass the central electron trigger (ELECTRON_CENTRAL_18) or the central muon triggers (MUON_CMUP18, MUON_CMX18). Due to trigger bandwidth limitations at high luminosity, several versions of the muon trigger: a luminosity-enabled version, which disables the CMX trigger until a certain luminosity is reached, a "JET10" version, which adds an additional jet requirement, and at the highest luminosities, one that combines the luminosity enable and jet requirement. The luminosity lost to the luminosity enabled CMX triggers is accounted for when the sample luminosity is calculated. Luminosities are calculated using the DQM version 18 good run list (bits [1,1,4,1]). The corresponding total integrated luminosity is $1.92\,\mathrm{fb}^{-1}$ for CEM and CMUP leptons and $1.88\,\mathrm{fb}^{-1}$ for CMX muons.

For the signal acceptance and systematic studies, $\rho_T^{\pm/0} \to W^{\pm}\pi_T^{0/\mp}$ samples are generated with PYTHIA 6.216 and simulated by the standard Monte Carlo procedure outlined in 6.1.4mc for each $\rho_T^{\pm/0}$and $\pi_T^{0/\mp}$mass. We set Q_U = 1 (charge of up-type technifermion), sinχ = 1/3 (χ is the mixing angle between isotriplet technipion interaction and mass eigenstates),M_V = M_A = 200 GeV (mass parameter for vector couplings and axial-vector). For the other Technicolor paramteres, we use the default setting of Pythia 6.216. Figure 2 and table 1-2 show $p\bar{p} \to \rho_T^{\pm/0} \to W^{\pm}\pi_T^{0/\mp}$ production cross section times branching ratio ($\pi_T^{0/\mp} \to b\bar{b}/b\bar{c}, b\bar{u}$) as a function of Technirho mass $m(\rho_T^{\pm/0})$ and Technipion mass $m(\pi_T^{0/\mp})$. The branching ratio of $\pi_T^0 \to b\bar{b}$ is about 83% for $m(\pi_T^0)$ = 95-165 GeV, and the branching ratio of $\pi_T^{\mp} \to b\bar{c}$ and $\pi_T^{\mp} \to b\bar{u}$ is about 55%, 36% for $m(\pi_T^{\mp})$ = 95-165 GeV. In this analysis, the mass points we focus on are: $m(\rho_T) > m(\pi_T) + m(W^{\pm})$ and $m(\rho_T) < 2 \times m(\pi_T)$.

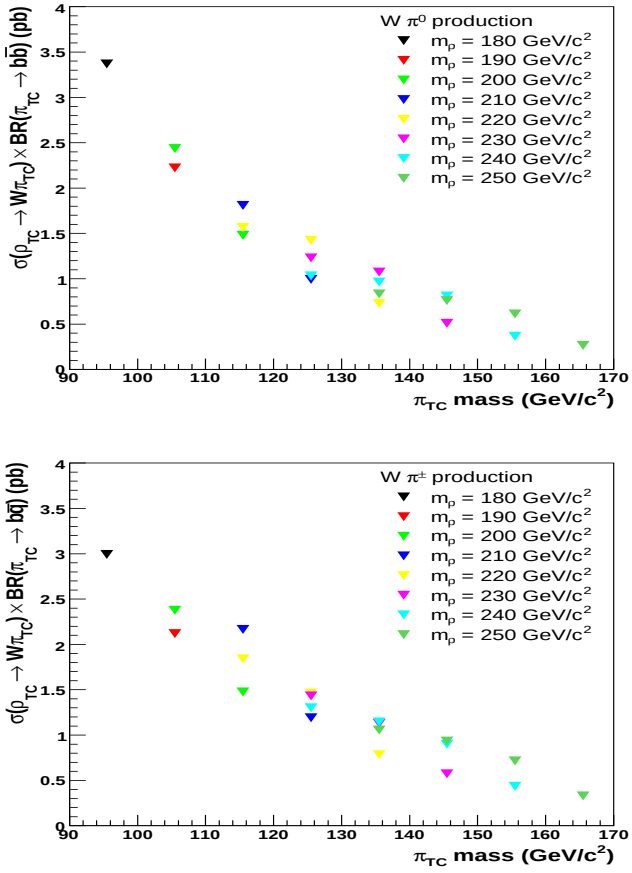

Figure 2: Top: $p\bar{p} \to \rho_T^{\pm} \to W^{\pm}\pi_T^0$ production cross section times Branching ratio ($\pi_T^0 \to b\bar{b}$) as a function of the Technipion mass ($m(\pi_T^0)$) for each Technirho mass ($m(\rho_T^{\pm})$). Bottom: $p\bar{p} \to \rho_T^0 \to W^{\pm}\pi_T^{\mp}$ production cross section times Branching ratio ($\pi_T^{\mp} \to b\bar{c}$ or $b\bar{u}$) as a function of the Technipion mass ($m(\pi_T^{\mp})$) for each Technirho mass ($m(\rho_T^0)$).

m($\rho_T^{\pm}$)/m(π_T^0)	95GeV	105GeV	115GeV	125GeV	135GeV	145GeV	155GeV	165GeV
180 GeV	3.37	—	—	—	—	—	—	—
190 GeV	—	2.22	—	—	—	—	—	—
200 GeV	—	2.44	1.48	—	—	—	—	—
210 GeV	—	—	1.81	0.99	—	—	—	—
220 GeV	—	—	1.57	1.42	0.73	—	—	—
230 GeV	—	—	—	1.23	1.07	0.51	—	—
240 GeV	—	—	—	1.03	0.96	0.81	0.37	—
250 GeV	—	—	—	—	0.83	0.76	0.61	0.27

Table 1: The production cross section of $\rho_T^{\pm} \to W^{\pm}\pi_T^0 \to W^{\pm}b\bar{b}$ (pb)

m(ρ_T^0)/m($\pi_T^{\mp}$)	95GeV	105GeV	115GeV	125GeV	135GeV	145GeV	155GeV	165GeV
180 GeV	2.99	—	—	—	—	—	—	—
190 GeV	—	2.12	—	—	—	—	—	—
200 GeV	—	2.38	1.48	—	—	—	—	—
210 GeV	—	—	2.16	1.19	—	—	—	—
220 GeV	—	—	1.84	1.46	0.79	—	—	—
230 GeV	—	—	—	1.43	1.13	0.57	—	—
240 GeV	—	—	—	1.30	1.15	0.90	0.43	—
250 GeV	—	—	—	—	1.06	0.93	0.72	0.33

Table 2: The production cross section of $\rho_T^0 \to W^{\pm}\pi_T^{\mp} \to W^{\pm}b\bar{c}, b\bar{u}$ (pb)

3 Event Selection

We use the exactly same event selection criteria as the WH search analysis [4]. We require the events to contain an isolated electron or muon with $E_T(p_T) > 20$ GeV as well as $\not\!\!E_T > 20$ GeV, after accounting for the muon and jet energy corrections. Jets are clustered using JETCLU with a cone size of 0.4 and are required to have $E_T > 20$ GeV after level 5 jet corrections (using `jetCorr12` jet energy correction code) and $|\eta_{Detector}| < 2.0$. Currently, we are not using any additional QCD veto, such as the standard cut on the angle between the $\not\!\!E_T$ and the leading jet. The tagged sample is defined by requiring that at least one of the jets has a positive tight SECVTX tag.

4 Neural Network b-tagging

The neural network b-tagger (NNBTAG) builds on the SECVTX secondary vertex tagger to separate the b jets from c and l (light) flavor jets. Jet variables which provide discrimination for b jets are combined into two neural networks. These networks are trained on and applied to events which have been already tagged by the SECVTX algorithm. A detailed description of the neural network training and validation is given in [5, 6]; neural network b-tagger is used by the WH search analysis and $\sim 10\%$ sensitivity is improved. Therefore, we also apply NN b-tagging in addition to SECVTX b-tgging because signal signature is same as WH and background components are identical. Here we summarize the most important features for the Technicolor search.

The tagger employs two neural networks in series. One is trained to separate b jets from light-flavor jets, and the other, b from c. Jets which pass a cut on both neural network output values are accepted by the tagger. These neural networks are trained and applied only to events which are already tagged by the SECVTX algorithm.

The neural networks take as input the same 16 variables. The following 8 variables are properties of the SECVTX tag: number of tracks, transverse decay length, transverse decay length significance, fit χ^2, pseudo-$c\tau$, vertex mass, vertex p_T divided by the sum of the good tracks' p_T, and vertex pass number. The following 8 variables are independent of the SECVTX vertex, but still have some power to discriminate b from c and l jets: number of good tracks, reconstructed mass of pass 1 tracks, reconstructed mass of pass 2 tracks, number of pass 1 tracks, number of pass 2 tracks, total p_T of pass 1 tracks divided by jet p_T, total p_T of pass 2 tracks divided by jet p_T, and jet probability value.

The network output spectra are well-modeled in our simulation. Figure 3 shows the neural network outputs from the $b-l$ network on a sample of SECVTX-tagged heavy-flavor jets from the 8-GeV electron sample and on a sample of tagged light-flavor jets from the jet-20 data.

We choose to set the cut value for 90% b efficiency (after the SECVTX efficiency), corresponding to a value of $NN_{bl} = 0.182$ and $NN_{bc} = 0.242$. The scale factor, measured from the electron sample in the `0h` and `0i` datasets, is 0.97 ± 0.02. (Note that this is the additional scale factor on top of the SECVTX scale factor, applicable because all of the jets under con-

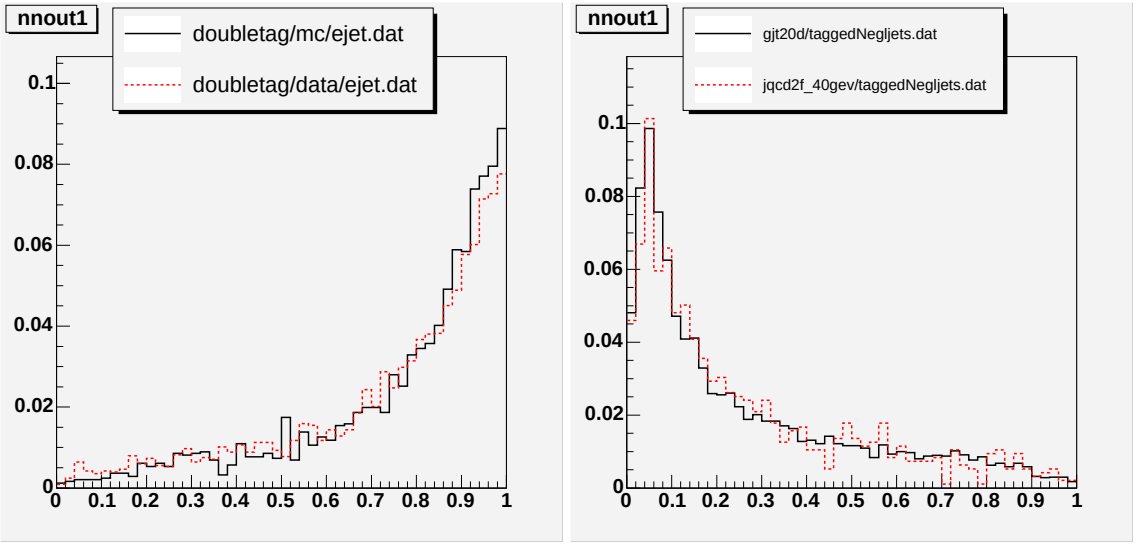

Figure 3: Comparisons of NN b-tag output in data and Monte Carlo for SECVTX-tagged heavy-flavor-enriched jets (left) and tagged light-flavor jets (right).

sideration have already been tagged by SECVTX). We have studied the jet rejection at these cut values, and find that we reject 65% of light-flavor jets and about 50% of the c jets.

We confirm Technicolor signal acceptance is able to keep 90% after applying NN b-tagging for each mass sample.

5 Background Estimation

The background components are based on WH search and $t\bar{t}$ lepton+jets cross section measurement analysis. The following backgrounds sources are considered in the W+jets sample:

Non-W QCD: A W signature is generated when one jet fakes a high p_T lepton and $\not\!\!E_T$ is generated through jet energy mismeasurement.

W + Mistags: This background occurs when one or more light flavor jets produced in association with a W boson are mistakenly identified as a heavy flavor jet by the b-tagging algorithms. Mistags are generated because of the finite resolution of the tracking, material interactions or long-lived light flavor hadrons (Λ and K_s) that produce displaced vertices.

W+ Heavy Flavor: These processes ($W + b\bar{b}$, $W + c\bar{c}$ and $W + c$) involve the production of actual heavy flavor quarks in association with a W boson.

Top Quark Backgrounds: This background comes both from single top quark production and top quark pair production.

Other EWK Backgrounds: Additional small background contributions come from Z + jets production and diboson (WW, WZ, and ZZ) production.

The Non-W background is estimated using the "MET vs ISO" technique described below, and use anti-electron as the Non-W background shape. The W + Mistag background is estimated from the data by applying a mistag parameterization, also known as the mistag matrix, to the data before tagging (pretag data). The W + Heavy Flavor background is also estimated from the pretag data using the ALPGEN + PYTHIA MC to set the relative normalization of light to heavy flavor events as well as the b-tagging efficiency for W + Heavy Flavor events (see below). The Top Quark and Other EWK backgrounds are normalized directly by their theoretical cross sections, calculated at next-to-leading order. More details can be found in the $t\bar{t}$ cross section documentation [7].

5.1 NonW(QCD fake) background

To estimate the number of events in which QCD jet fakes a lepton, we use the $\not\!\!E_T$ vs Isolation method. We divide the $\not\!\!E_T$ vs isolation plane into the following regions (see Figure 4):

- region A: Isolation $>$ 0.2 and $\not\!\!E_T < 15$ GeV
- region B: Isolation $<$ 0.1 and $\not\!\!E_T < 15$ GeV
- region C: Isolation $>$ 0.2 and $\not\!\!E_T > 20$ GeV
- region D: Isolation $<$ 0,1 and $\not\!\!E_T > 20$ GeV

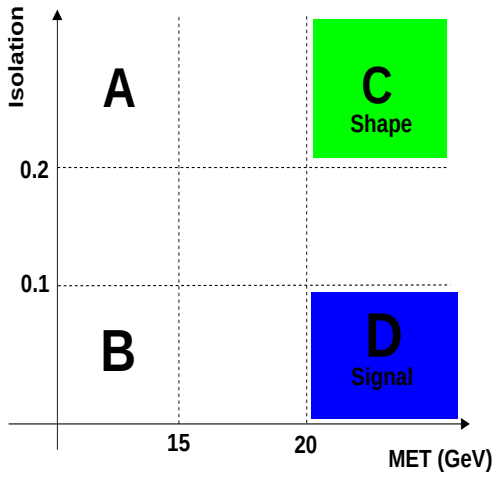

Figure 4: Each region in $\not\!\!E_T$ and lepton isolation plane

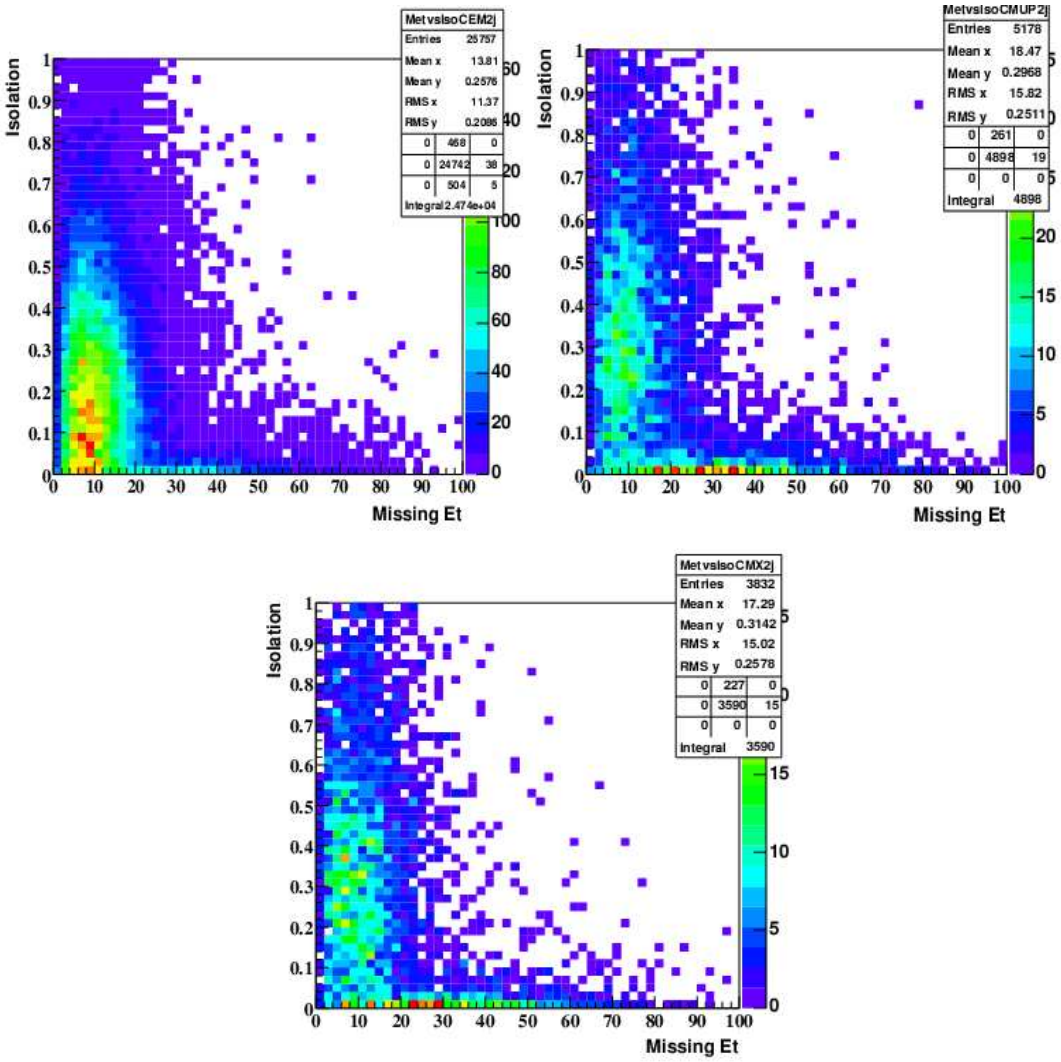

Figure 5: Observed data on $\not\!\!E_T$ vs Iso plane. From left, CEM, CMUP and CMX region. These events has exact 2 tight jets

Here region D is our signal region. We assume that the lepton isolation is independent of $\not\!\!E_T$, and that the tagging efficiency is the same between Region B and D. Then we define the fraction of events which are the non-W contribution:

$$f_{\text{non}-W} = \frac{N_B \times N_C}{N_A \times N_D}, \tag{1}$$

where N_i $(i = A, B, C, D)$ are the number of pretag events in each sideband region. To obtain the non-W background for tagged events, we measure the b-tagging efficiency from

region B. For this purpose, we define tagging efficiency as

$$r_B = \frac{N_B^{(\text{tagged events})}}{N_B^{(\text{taggable jets})}}, \tag{2}$$

where $N_B^{(\text{tagged jets})}$ and $N_B^{(\text{taggable jets})}$ are number of taggable and tagged jets in region B respectively. Then we obtain the non-W background in region D with the relation

$$N_D^{(\text{non}-W)} = f_{\text{non}-W} \times r_B \times N_D^{(\text{taggable jets})}. \tag{3}$$

We call this procedure the "Tag Rate Method" since it uses the tag rate in region B. It is also possible to have a estimate directly from the tagged sample, by using

$$N_D^+ = \frac{N_B^+ \times N_C^+}{N_A^+}, \tag{4}$$

where $+$ denotes positive tagged events, and we call this method as "Tagged Method" in this note.

These methods are data-based techniques, so the estimates could also contain other background processes. Subtracting the known backgrounds should result in a better non-W QCD estimate. The contributions from $t\bar{t}$ and W+jets events to each sideband region are estimated and subtracted based on theoretical cross section and ratio to D region. The non-W fractions after the correction are shown in Table 3. Systematic uncertainty of nonW fraction ,25%, are quoted from previous analysis[3],[4] as there are no reason to change from previous. To combine the estimates from the tag rate and tagged methods, the two sums are combined in a weighted average to get the total non-W backgrounds.

The low statistics of the double-tagged and NN tagged samples prevents us from applying this technique directly. Instead, estimates from the $\geq$ 1-tagged sample are extended into the double-tagged or NN tagged sample using the ratio of at events with at least 1 tag to events with double tag events in region A'(Isolation > 0.1 and $10 < \not\!\!E_T < 20$ GeV), B, and C'(Isolation > 0.1 and $\not\!\!E_T > 20$ GeV).

5.2 W + Heavy flavor

The $Wb\bar{b}$ and $Wc\bar{c}$ states are major sources of background of b-tags in the W+jets channel. They are estimated primarily from the Monte Carlo, but their overall rates are normalized to data. The contribution from true heavy flavor production in W+jet events is determined from measurements of the heavy flavor event fraction in W+jet events and the tagging efficiency for those events. These heavy flavor fractions and a scaling factor for these fractions (k-factor) have been studied extensively elsewhere [7, 8] using ALPGEN v2 + PYTHIA Monte Carlo. Heavy flavor fractions measured in ALPGEN have been calibrated using a W+1jet data sample, and it is found that a k-factor of 1.4 ± 0.4 is necessary to make the heavy flavor production in Monte Carlo match the production in data. Although we can apply most of the numbers from [7] without modification, we need to calculate the tagging efficiency of the

Njets	1jet	2 jet	>= 3jet
bhel0d	0.209±0.052	0.232±0.059	0.248±0.065
bhmu0d	0.055±0.014	0.071±0.018	0.090±0.025
bhel0h	0.236±0.059	0.251±0.063	0.251±0.065
bhmu0h	0.056±0.014	0.067±0.017	0.058±0.016
bhel0i	0.246±0.062	0.260±0.066	0.215±0.057
bhmu0i	0.054±0.014	0.071±0.018	0.073±0.021
bhelmi (Period 8)	0.257±0.065	0.264±0.067	0.280±0.075
bhmumi (Period 8)	0.054±0.014	0.072±0.019	0.078±0.023
bhelmi2 (Period 9)	0.258±0.065	0.291±0.074	0.256±0.069
bhmumi2 (Period 9)	0.057±0.014	0.065±0.017	0.061±0.019
bhelmi3 (Period 10)	0.275±0.069	0.277±0.070	0.308±0.081
bhmumi3 (Period 10)	0.059±0.015	0.073± 0.019	0.038±0.011
bhel0j (Period 11)	0.287±0.072	0.285± 0.072	0.84±0.075
bhmu0j (Period 11)	0.055±0.014	0.080±0.021	0.068±0.020
bhelmj2 (Period 12)	0.279±0.07	0.287± 0.073	0.285±0.077
bhmumj2 (Period 12)	0.059±0.015	0.075±0.020	0.068±0.021

Table 3: NonW fraction after correction for each dataset and each jet bin. 3 jet and more than 3 jet is merged due to statistical limitation

One SECVTX w/ NN tag	1jet	2 jet	3 jet	>=4 jet
WBB (1B)	27.5±1.49	28.1±1.25	26.7±1.42	26.9± 3.67
WBB (2B)		26.2±1.22	24.1±1.23	22.6±1.31
WCC (1C)	4.17±0.23	4.59±0.25	4.91±0.29	5.23±0.66
WCC (2C)		6.28±0.38	6.56±0.42	6.85±0.64

Table 4: Heavy flavor tagging efficiency calculated from ALPGEN v2 W+jets MC for one SECVTX w/ NNtag category.

ST+JP and one SECVTX tag w/ NNtag categories ourselves. Table 4,5 show the heavy flavor tagging efficiency results for these two categories. The heavy flavor fractions and tagging efficiencies are multiplied by the number of pre-tagged events in data, after the number of pre-tagged events has been corrected for the non-W and other background contribution.

$$N_{W+HF} = f_{HF} \cdot \epsilon_{\rm tag} \cdot [N_{\rm pretag} \cdot (1 - f_{\rm non-W}) - N_{\rm EWK}] \,, \tag{5}$$

where f_{HF} is heavy fraction, $\epsilon_{\rm tag}$ is tagging efficiency and $N_{\rm EWK}$ is the expected number of $t\bar{t}$ and diboson events.

SECVTX + Jet Probability(5%)	2 jet	3 jet	>=4 jet
WBB (2B)	10.1±1.2	11.1±1.3	12.4±1.5
WCC (2C)	1.6±0.2	2.3±0.3	3.2±0.4

Table 5: Heavy flavor tagging efficiency calculated from ALPGEN v2 W+jets MC for double b-tagging categories.

5.3 Mistag

The rate of W + mistag, or falsely tagged jets, is derived from a sample of events collected with a jet-based trigger with no heavy flavor requirement. The mistag rate is obtained using negative tags, which are the tags that appear to travel back toward the primary vertex. The mistag rate obtained from negative tags is parameterized in bins of η, jet E_T, track multiplicity within a jet, $\sum E_T$ of the event, number of z vertices, and the z vertex position [13]. The mistag rate derived from negative tags is corrected for the effects of heavy flavor in the jet sample, long-lived light flavor vertices, and vertices caused by material interactions in the silicon detector. This correction is parameterized as a function of E_T to reduce its systematic uncertainty [9].

Tag rate probabilities for events with at least one SECVTX tag are obtained by summing over all of the taggable jets in pretag events and exact one tag events. For double tagged events, we apply a similar procedure to events with exactly one tight SECVTX tag, summing tag rate probabilities for all taggable jets except the tagged one. The total mistag normalization is obtained by adding up all the mistag probability event sums for the pretag events. Figure 6 illustrates our mistag background calculation scheme.

The uncertainty on the mistag estimate includes the statistical errors from the matrix itself, accounting for correlations between jets which fall in the same bin of the mistag matrices, and an additional 5.9% error from all systematic uncertainties [13]. Although the mistag matrix was derived using the 1.12fb^{-1} sample, it has been shown that it is acceptable to apply this at least through period 12 data as long as the systematic uncertainties are increased by 1.8% to cover possible discrepancies.

For jet probability, mistag matrix is applied like SECVTX tag. This matrix is parametrized in E_T ,η, ϕ of jet, Number of track, sumE_T , z vertex position. To estimate the mistag backgrounds for ST+JP category, we use the dedicated mistag matrix for SecVtx + Jet Probability category.

For NN b-tagging, we apply rejection factor 0.65±0.05 to one SECVTX tagged events estimated in [5]

5.4 MC derived background

The normalization of the diboson, $t\bar{t}$ and single top backgrounds are based on the theoretical cross sections (listed in Table 6), the measured luminosity and the acceptance and b-tagging efficiency derived from MC. The MC acceptance is corrected for lepton identification, trigger

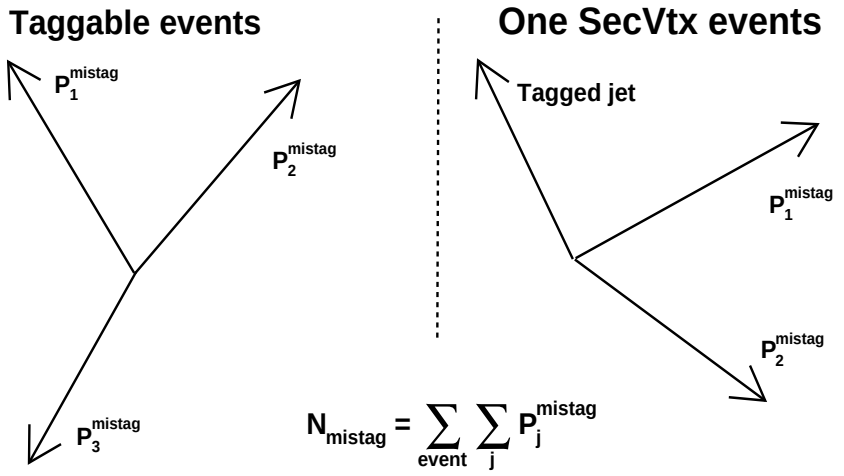

Figure 6: Mistag calculation in each tag

Theoretical Cross Sections	
WW	12.4 ± 0.25 pb
WZ	3.96 ± 0.06 pb
ZZ	1.58 ± 0.05 pb
Single Top s-channel	0.88 ± 0.11 pb
Single Top t-channel	1.98 ± 0.25 pb
$Z \rightarrow \tau\tau$	265 ± 30.0 pb
$t\bar{t}$	$6.7\ ^{+0.7}_{-0.9}$ pb

Table 6: Theoretical cross sections and errors for the electroweak and single top backgrounds, along with the theoretical cross section for $t\bar{t}$ at ($m_t = 175$GeV/c^2). The cross section of $Z^0 \rightarrow \tau\tau$ is obtained from direct CDF measurement.

efficiencies and z vertex cut. The tagging efficiency is always scaled by the MC/data scale factor of 0.95$\pm$ 0.05 for SECVTX and 0.85$\pm$0.07 for jet probability. For NN b-tag, the tagging efficiency is scaled by the factor 0.97$\pm$0.02. The expected number of events is obtained by the equation

$$N = \int \mathcal{L}dt \times \epsilon \times \sigma, \tag{6}$$

where ϵ is the total detection efficiency corrected by all of the scale factors.

Njet	1jet	2jet	3jet	>=4jet
Pretag Events	196160	32242	5496	1494
Mistag	236.7±19.36	107.1±9.38	41.84±3.839	20.97±1.91
$Wb\bar{b}$	431.7±182.4	215.6±92.34	61.78±24.68	26.14±10.43
$Wc\bar{c}$	514.4±154.7	167±62.14	45.4±15.31	17.71±6.86
$t\bar{t}$(6.7pb)	11.85±1.82	60.68±9.30	111±17.03	122.4±18.76
Single top(s-ch)	7.09±1.03	14.38±2.09	3.91±0.57	0.97±0.14
Single top(t-ch)	23.31±3.41	29.57±4.33	6.24±0.91	1.11±0.16
WW	7.21±0.89	15.45±1.91	4.61±0.57	1.03±0.13
WZ	5.52±0.59	7.59±0.81	1.76±0.19	0.48±0.05
ZZ	0.17±0.02	0.31±0.03	0.14±0.01	0.07±0.01
$Z->\tau\tau$	14.58±2.25	7.27±1.12	2.39±0.37	0.71±0.11
nonW QCD	465±83.21	184.7±33.04	44.83±8.57	17.03±3.67
Total Bkg	1717.6±347.89	809.61±159.38	323.92±45.45	208.57±26.24
m($\rho^{\pm}$,π^0)=(200,115) GeV	Control region	20.74 ± 1.61	Control region	Control region
m(ρ^0,$\pi^{\mp}$)=(200,115) GeV	Control region	22.96±1.78	Control region	Control region
Observed Events	1812	805	306	215

Table 7: Background summary table for one tag w/ NNtag category

5.5 Background summary

We have described the contributions of individual background sources to the final background estimate. The summary of the background estimates for each tag category are shown in table 7 - 9.

Njet	2jet	3jet	>=4jet
Pretag Events	32242	5496	1494
Mistag	3.88±0.35	2.41±0.24	1.62± 0.14
$Wb\bar{b}$	37.93±16.92	14.05±5.49	7.39± 2.93
$Wc\bar{c}$	2.88±1.25	1.52±0.61	1.15± 0.47
$t\bar{t}$(6.7pb)	19.05±2.92	54.67±8.38	94.93± 14.56
Single top(s-ch)	6.90±1.00	2.28±0.33	0.61± 0.088
Single top(t-ch)	1.60±0.23	1.43±0.21	0.50± 0.07
WW	0.17±0.02	0.15±0.02	0.16± 0.02
WZ	2.41±0.26	0.68±0.07	0.16± 0.02
ZZ	0.06±0.01	0.06±0.01	0.02±0.001
$Z->\tau\tau$	0.25±0.04	0.19±0.03	0.06±0.01
nonW QCD	5.50±1.00	2.56±0.48	1.02± 0.22
Total Bkg	80.62±18.75	79.99±10.92	107.63± 15.15
m($\rho^{\pm}$,π^0)=(200,115) GeV	11.24±0.98	Control region	Control region
m(ρ^0,$\pi^{\mp}$)=(200,115) GeV	1.50±0.16	Control region	Control region
Observed Events	83	88	118

Table 8: Background summary table for double SECVTX tag category

Njet	2jet	3jet	>=4jet
Pretag Events	32242	5496	1494
Mistag	11.73±0.92	8.11±0.64	8.39±0.58
$Wb\bar{b}$	31.15±14.03	11.47±4.55	6.55±2.63
$Wc\bar{c}$	7.87±3.43	4.38±1.76	3.09±1.27
$t\bar{t}$(6.7pb)	15.56±2.39	47.48±7.28	79.81±12.24
Single top(s-ch)	5.14±0.75	1.90±0.27	0.53±0.07
Single top(t-ch)	1.87±0.27	1.49±0.22	0.44±0.06
WW	0.93±0.11	0.63±0.08	0.47±0.06
WZ	1.84±0.20	0.59±0.06	0.19±0.02
ZZ	0.08±0.01	0.04±0.003	0.02±0.002
$Z->\tau\tau$	1.29±0.20	0.53±0.08	0.20±0.03
nonW QCD	9.55±1.73	4.87±0.93	1.80±0.40
Total Bkg	86.99±17.99	81.46±10.22	101.49±13.08
m($\rho^{\pm}$,π^0)=(200,115) GeV	7.69±0.87	Control region	Control region
m(ρ^0,$\pi^{\mp}$)=(200,115) GeV	2.85±0.34	Control region	Control region
Observed Events	90	80	106

Table 9: Background summary table for one SECVTX tag + Jet Probability tag category

6 Technicolor Signal Acceptance

6.1 Introduction

To calculate the expected number of signal events $N_{\rho_T \to \pi_T W \to l\nu b\bar{q}(\bar{q}=\bar{b},\bar{c},\bar{u})}$, the following equation is used:

$$N_{\rho_T \to \pi_T W \to l\nu b\bar{q}} = \epsilon_{\rho_T \to W\pi_T \to l\nu b\bar{q}} \cdot \mathcal{L} \cdot \sigma(p\bar{p} \to \rho_T \to \pi_T W^{\pm}) \cdot BR(\pi_T \to b\bar{q}), \qquad (7)$$

where, $\epsilon_{\rho_T \to W\pi_T \to l\nu b\bar{q}}$ is detection efficiency for signal, $\mathcal{L}$ is the integrated luminosity, $\sigma(p\bar{p} \to \rho_T \to \pi_T W^{\pm})$ is the Technicolor production cross section in proton antiproton collisions and $BR(\pi_T \to b\bar{q})$ is branching ratio for π_T decaying to $b\bar{q}$. The detection efficiency for signal events is defined as:

$$\epsilon_{\rho_T \to W\pi_T \to l\nu b\bar{q}} = \epsilon_{Z0} \cdot \epsilon_{trig} \cdot \epsilon_{leptonid} \cdot \epsilon^{MC}_{W\pi_T \to l\nu b\bar{q}} \cdot \left(\sum_{l'=e,\mu,\tau} BR(W \to l'\nu) \right), \qquad (8)$$

where $\epsilon^{MC}_{W\pi_T \to l\nu b\bar{q}}$ is the fraction of signal events (with $|z_0| < 60$cm) which pass the kinematic and b-tagging requirements. The effect of the b-tagging scale factor in this fraction is included by randomly selecting tagged jets to discard. The quantity ϵ_{Z0} is efficiency of the $|z_0| < 60$ cm cut, and is measured in data. The trigger efficiencies for high p_T leptons, ϵ_{trig}, are also measured in data using back-up triggers with looser requirements [10, 12]. The lepton id and reconstruction efficiencies measured in Monte Carlo are corrected by scale factors, $\epsilon_{leptonid}$ derived from data [11, 12]. Finally, $Br(W \to l'\nu)$ is the branching ratio for leptonic W decay. Each of these factors and their systematic errors are treated separately for each data period and the results are combined weighted by the luminosity of each data period. For the later data periods, where numbers may not have been finalized, preliminary results have been taken from the slides of talks given in the Joint Physics meeting [14].

We generate the Technicolor samples with 180-210 GeV for $m(\rho_T^{\pm/0})$ and 95-125 GeV for $m(\pi_T^{0/\mp})$. These samples are used to estimate Technicolor signal MC efficiency and systematic uncertainty. Figure 7-10 show the overall acceptance as a function of $m(\pi_T^{0/\mp})$ for each $m(\rho_T^{\pm/0})$ in exact 1 SECVTX tag with NN tag, double SECVTX tag and one SECVTX tag + one jet probability tag. In these figures systematic uncertainties are included in error bar. Signal systematic uncertainty is discussed in the following subsection in detail.

The expected number of Technicolor signal events are estimated from the calculated acceptance at each mass. The expected number for each event selection and for each mass points are shown in Tables 10 and 11. In these tables expected events are calculated from 2 jet bin only.

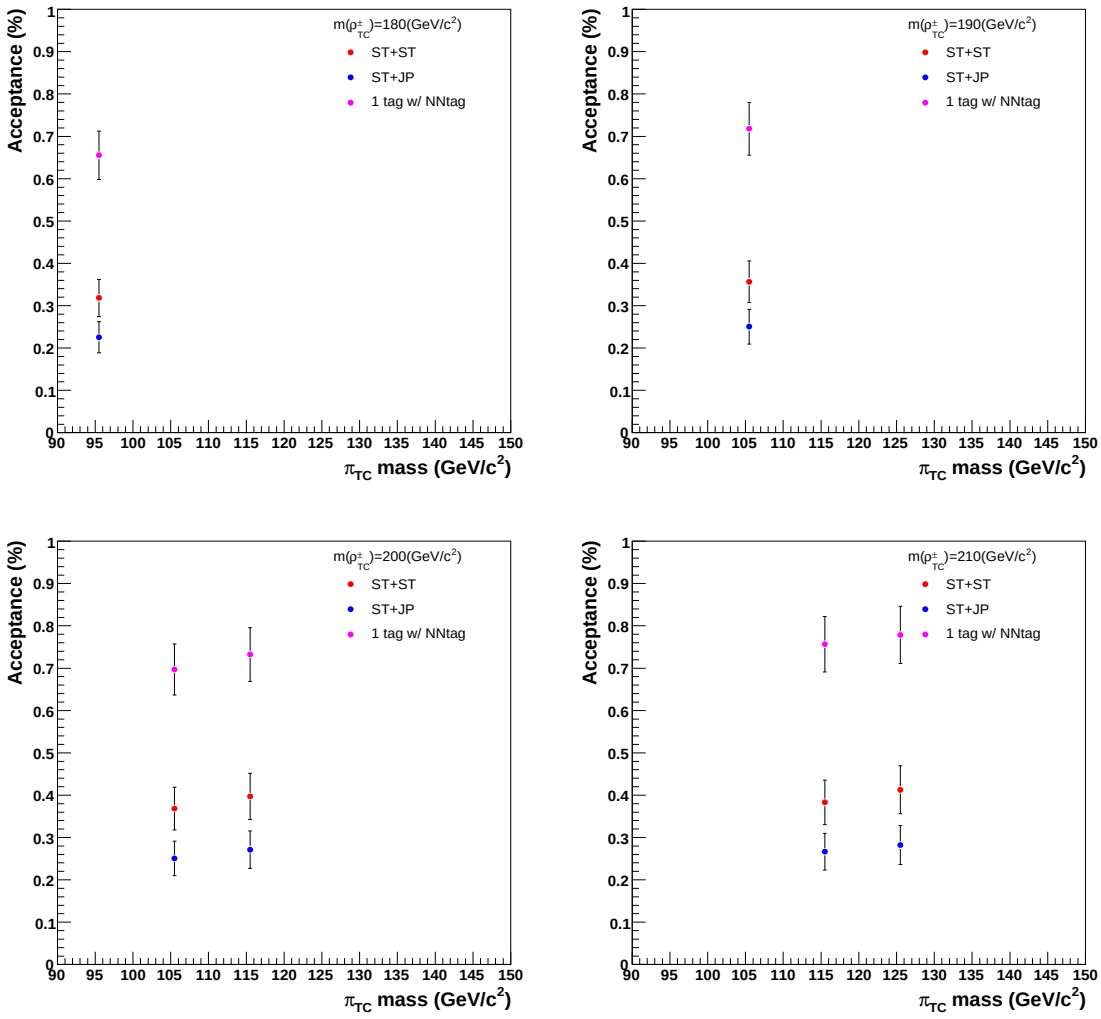

Figure 7: The Technicolor signal acceptance as a function of Technipi mass ($m(\pi_T^0)$) for each Techinirho mass ($m(\rho_T^{\pm})$) in exact one secVtx tag with NN b-tagging, double SECVTX tag and one SECVTX tag + one jet probability tag. From top left ($m(\rho_T^{\pm})$=180 GeV, 190 GeV, 200 GeV and 210 GeV.

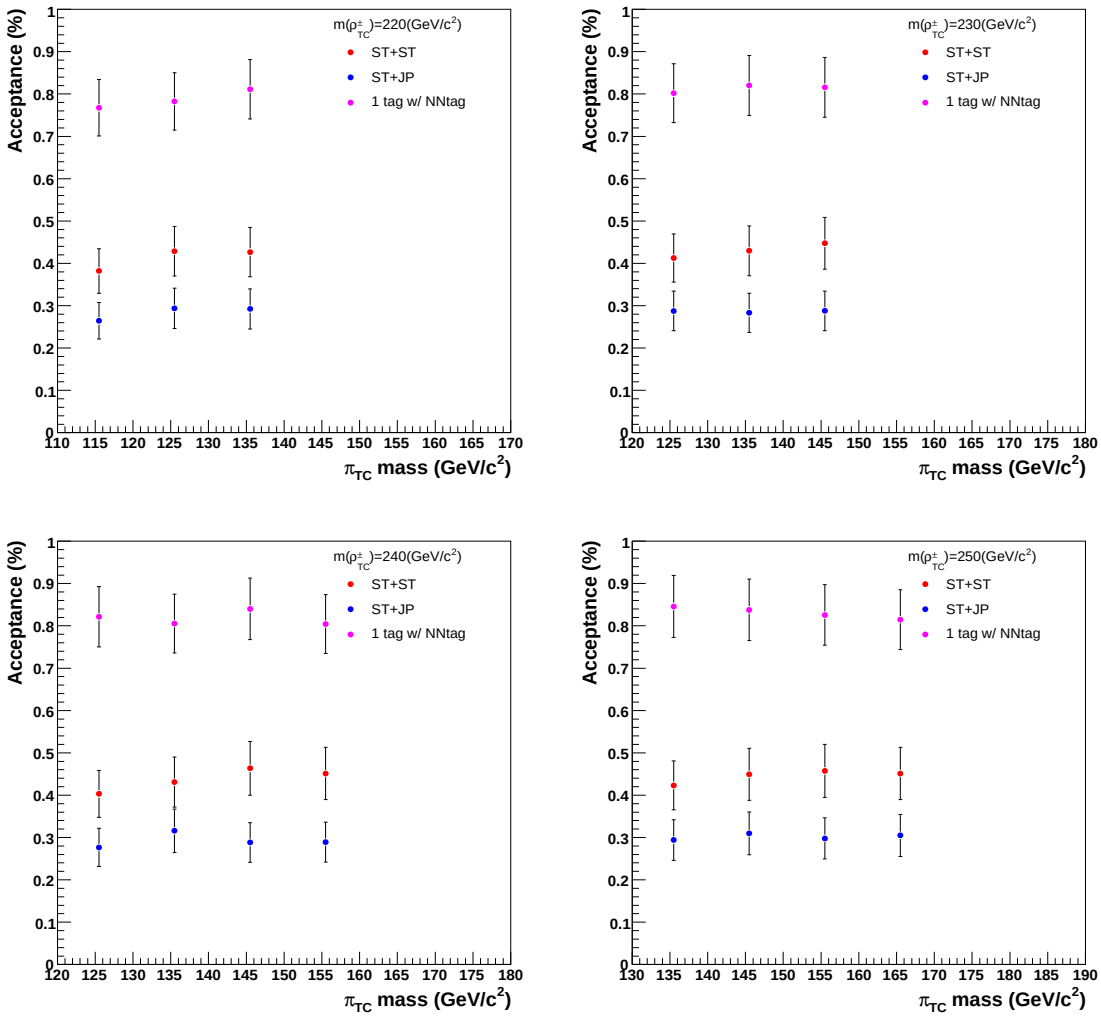

Figure 8: The Technicolor signal acceptance as a function of Technipi mass ($m(\pi_T^0)$) for each Techinirho mass ($m(\rho_T^{\pm})$) in exact one secVtx tag with NN b-tagging, double SECVTX tag and one SECVTX tag + one jet probability tag. From top left ($m(\rho_T^{\pm})$=220 GeV, 230 GeV, 240 GeV and 250 GeV.

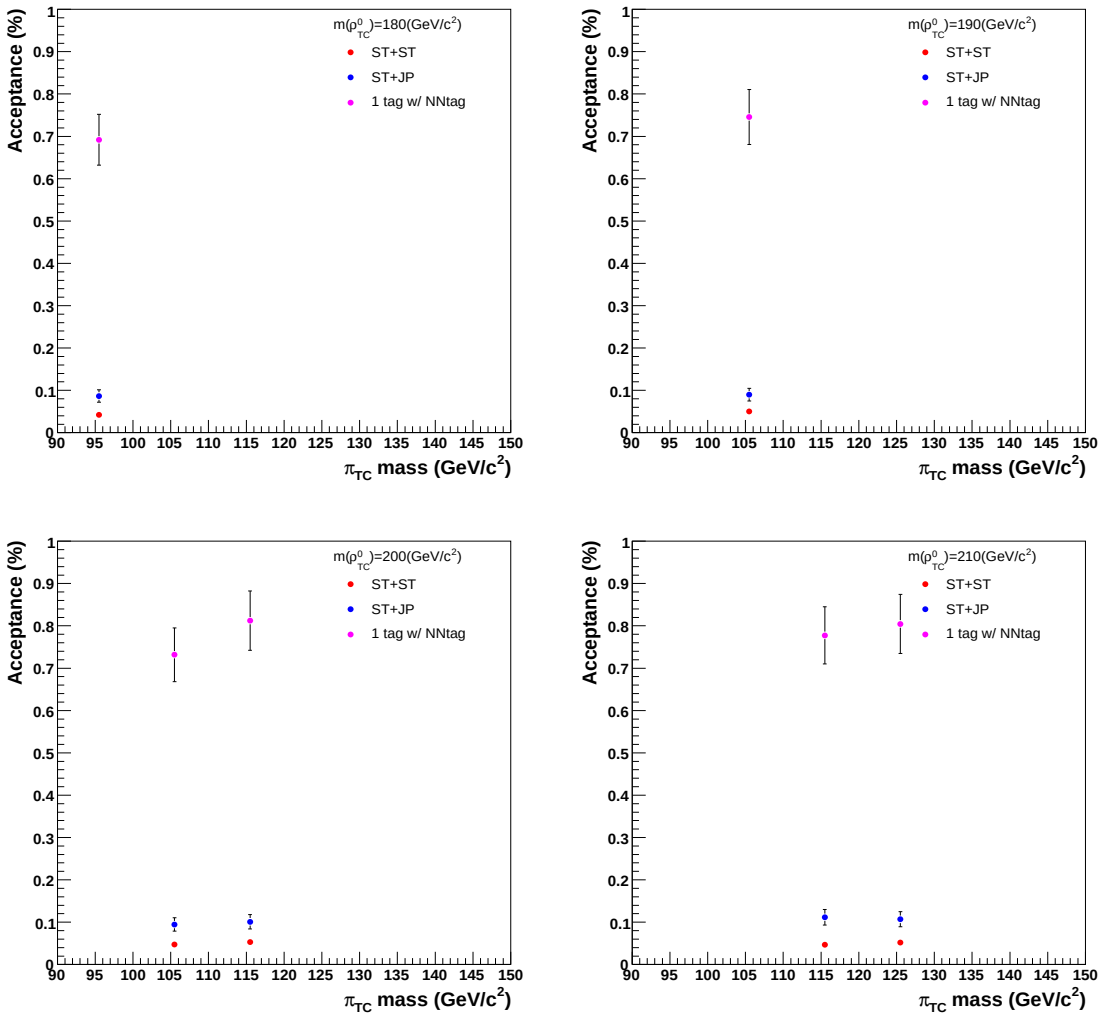

Figure 9: The Technicolor signal acceptance as a function of Technipi mass ($m(\pi_T^{\mp})$) for each Techinirho mass ($m(\rho_T^0)$) in exact one secVtx tag with NN b-tagging, double SECVTX tag and one SECVTX tag + one jet probability tag. From top left ($m(\rho_T^0)$=180 GeV, 190 GeV, 200 GeV and 210 GeV.

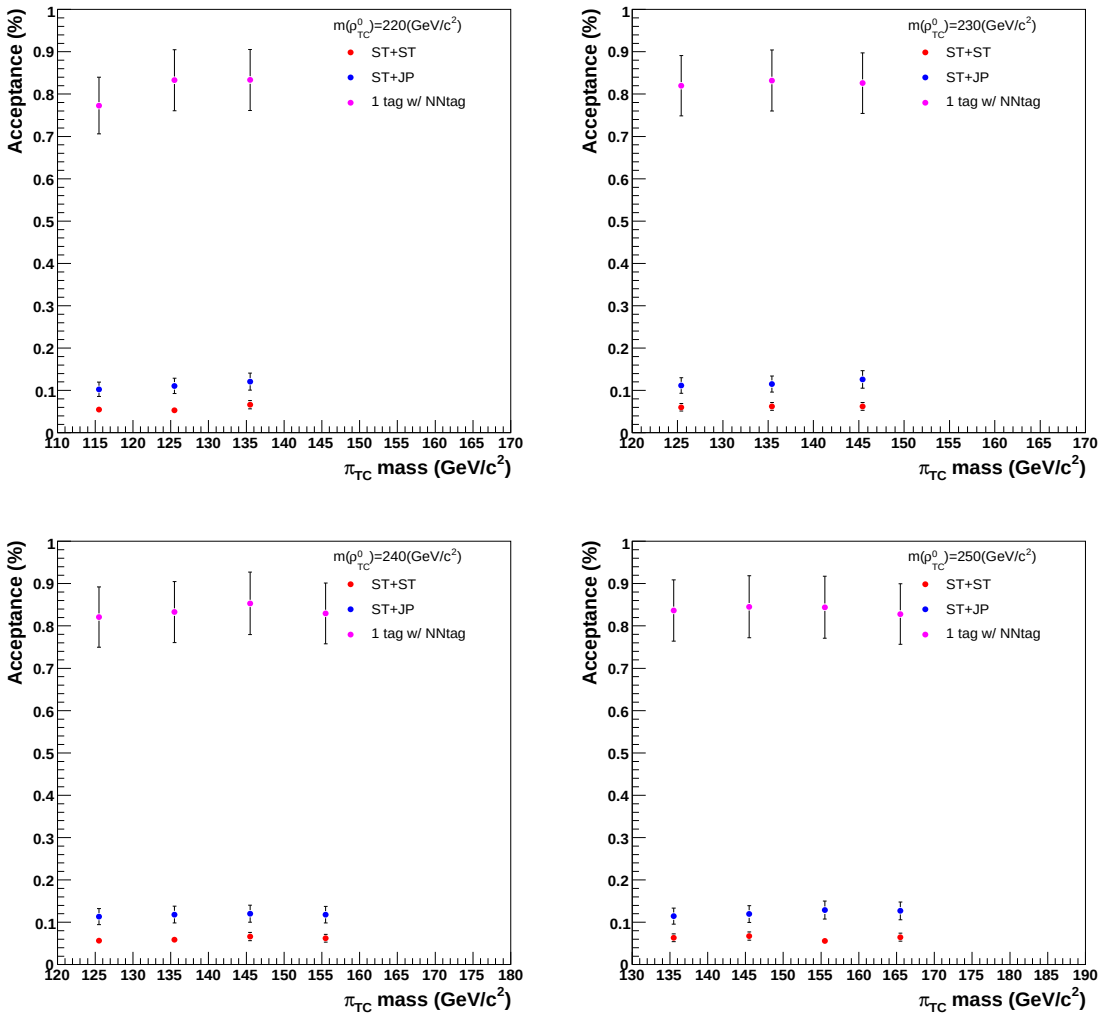

Figure 10: The Technicolor signal acceptance as a function of Technipi mass ($m(\pi_T^{\mp})$) for each Techinirho mass ($m(\rho_T^0)$) in exact one secVtx tag with NN b-tagging, double SECVTX tag and one SECVTX tag + one jet probability tag. From top left ($m(\rho_T^0)$=220 GeV, 230 GeV, 240 GeV and 250 GeV.

Expected Technicolor events			
$m(\rho_T^{\pm},\pi_T^0)$	1tag w/ NNtag	ST+ST	ST+JP
(180,95)	42.29 +/- 3.30	20.53 +/- 1.81	14.53 +/- 1.65
(190,95)	30.59 +/- 2.38	15.19 +/- 1.33	10.66 +/- 1.21
(200,105)	32.52 +/- 2.54	17.19 +/- 1.51	11.70 +/- 1.33
(200,115)	20.74 +/- 1.62	11.24 +/- 0.98	7.69 +/- 0.87
(210,115)	26.24 +/- 2.04	13.28 +/- 1.16	9.24 +/- 1.05
(210,125)	14.83 +/- 1.15	7.86 +/- 0.69	5.37 +/- 0.61
(220,125)	23.02 +/- 1.79	11.46 +/- 1.00	7.93 +/- 0.90
(220,135)	21.35 +/- 1.66	11.69 +/- 1.02	8.01 +/- 0.90
(220,145)	11.30 +/- 0.88	5.94 +/- 0.52	4.07 +/- 0.46
(230,125)	18.90 +/- 1.47	9.72 +/- 0.85	6.77 +/- 0.77
(230,135)	16.88 +/- 1.31	8.84 +/- 0.77	5.83 +/- 0.66
(230,145)	7.94 +/- 0.62	4.35 +/- 0.38	2.80 +/- 0.32
(240,125)	16.26 +/- 1.26	7.98 +/- 0.70	5.47 +/- 0.62
(240,135)	14.88 +/- 1.16	7.96 +/- 0.69	5.84 +/- 0.66
(240,145)	13.02 +/- 1.01	7.18 +/- 0.62	4.47 +/- 0.50
(240,155)	5.62 +/- 0.44	3.16 +/- 0.27	2.02 +/- 0.23
(250,135)	13.50 +/- 1.05	6.75 +/- 0.59	4.69 +/- 0.53
(250,145)	12.20 +/- 0.95	6.54 +/- 0.57	4.51 +/- 0.51
(250,155)	9.70 +/- 0.75	5.37 +/- 0.47	3.50 +/- 0.39
(250,165)	4.14 +/- 0.32	2.29 +/- 0.20	1.55 +/- 0.17

Table 10: The expected technicolor signal of the $\rho_T^{\pm} \to W^{\pm}\pi_T^0 \to l\nu b\bar{b}$ process.

Expected Technicolor events			
$m(\rho_T^0,\pi_T^{\mp})$	1tag w/ NNtag	ST+ST	ST+JP
(180,95)	39.66 +/- 3.09	2.41 +/- 0.26	4.96 +/- 0.59
(190,95)	30.29 +/- 2.36	2.03 +/- 0.21	3.65 +/- 0.43
(200,105)	33.33 +/- 2.60	2.16 +/- 0.23	4.30 +/- 0.51
(200,115)	22.96 +/- 1.78	1.50 +/- 0.16	2.85 +/- 0.34
(210,115)	32.24 +/- 2.51	1.93 +/- 0.20	4.63 +/- 0.54
(210,125)	18.38 +/- 1.43	1.18 +/- 0.12	2.44 +/- 0.29
(220,125)	27.27 +/- 2.12	1.94 +/- 0.20	3.62 +/- 0.43
(220,135)	23.36 +/- 1.81	1.49 +/- 0.16	3.11 +/- 0.36
(220,145)	12.54 +/- 0.98	1.00 +/- 0.10	1.82 +/- 0.21
(230,125)	22.49 +/- 1.75	1.65 +/- 0.17	3.06 +/- 0.36
(230,135)	17.98 +/- 1.40	1.35 +/- 0.14	2.49 +/- 0.29
(230,145)	9.07 +/- 0.70	0.69 +/- 0.07	1.38 +/- 0.16
(240,125)	20.48 +/- 1.59	1.41 +/- 0.15	2.83 +/- 0.33
(240,135)	18.27 +/- 1.42	1.29 +/- 0.13	2.59 +/- 0.30
(240,145)	14.71 +/- 1.14	1.14 +/- 0.11	2.07 +/- 0.24
(240,155)	6.90 +/- 0.54	0.52 +/- 0.05	0.98 +/- 0.11
(250,135)	16.91 +/- 1.31	1.28 +/- 0.13	2.32 +/- 0.27
(250,145)	15.11 +/- 1.17	1.20 +/- 0.12	2.13 +/- 0.25
(250,155)	11.58 +/- 0.90	0.77 +/- 0.08	1.76 +/- 0.21
(250,165)	5.24 +/- 0.41	0.41 +/- 0.04	0.80 +/- 0.09

Table 11: The expected technicolor signal of the $\rho_T^0 \to W^{\pm}\pi_T^{\mp} \to l\nu b\bar{c}, b\bar{u}$ process.

b-tagging category	LeptonID	Trigger	ISR/FSR	JES	PDF	b-tagging	Total
One tag w/ NN tag	$\sim 2\%$	$< 1\%$	2.4/1.8%	2.7%	2.3%	4.3%	6.7%
ST + ST	$\sim 2\%$	$< 1\%$	5.5/3.0%	3.8%	3.4%	8.4%	11.9%
ST + JP	$\sim 2\%$	$< 1\%$	4.6/3.3%	4.0%	3.6%	9.2%	12.2%

Table 12: Systematic uncertainties for π_T^0 channel for each tagging category

b-tagging category	LeptonID	Trigger	ISR/FSR	JES	PDF	b-tagging	Total
One tag w/ NN tag	$\sim 2\%$	$< 1\%$	3.2/2.3%	3.4%	3.0%	4.3%	7.7%
ST + ST	$\sim 2\%$	$< 1\%$	11.6/8.3%	11.3%	3.8%	9.4%	21.0%
ST + JP	$\sim 2\%$	$< 1\%$	8.0/5.1%	5.9%	3.8%	17.0%	20.8%

Table 13: Systematic uncertainties for $\pi_T^{\mp}$ channel for each tagging category

6.2 Systematic Uncertainties on Acceptance

The systematic uncertainties on the acceptance derive from the jet energy scale, initial and final state radiation, lepton ID and trigger efficiencies and the b-tagging scale factor. To obtain the systematic uncertainty from jet energy scale, we use the Technicolor sample of the mass ($m(\rho_T)$ = 200, $m(\pi_T)$ = 115 GeV/c^2). The jet energies in the Technicolor MC samples are shifted by $\pm 1\sigma$ and the difference from the nominal acceptance is taken as a systematic uncertainty.

Lepton ID and trigger systematics are estimated in [10, 11, 12, 14]. These systematics uncertainties are calculated for each run range and combined using a luminosity weighted average. $\sim$ 2% is assigned as Lepton ID systematic uncertainty. The uncertainty for the trigger efficiency is estimated to be less than one percent.

ISR and FSR systematic uncertainty are estimated by changing the parameters related to ISR and FSR from default values to half and double. Half of difference between the two samples is taken as the systematic uncertainly.

PDFs uncertainties are evaluated using the standard re-weighting method recommended by Joint Physics [14].

The b-tagging scale factor uncertainty comes from the High p_T b-tagging group.

Propagating these uncertainties through our analysis, we estimate the final acceptance uncertainties for one SECVTX tag w/ NN tag, double SECVTX tag and one SECVTX plus Jet Probablity. Total systematic uncertainties are listed in table 12 and 13 for each b-tagging category.

Luminosity uncertainties are also included in calculating Technicolor signal events. This uncertainty is assigned as 6%.

Note: Previous versions of WH analysis suggest that the acceptance systematics are much larger than the shape systematics. Therefore, at this time, we've focused on the acceptance systematics. In the near future, we will check this assumption by evaluating shape systematics.

7 Neutrino solution procedure and reconstructed mass distribution

We perform a direct search for a resonant mass peak in the reconstructed $W^{\pm}+2$ jet and dijet invariant mass distributions with level 5 jet energy correction. To reconstruct the $W^{\pm}+2$ jets mass, we need to determine the p_z of neutrino from $W^{\pm}$ boson. In this analysis we apply same procedure of determining the p_z of neutrino as previous analysis [2]. We use $W^{\pm}$ mass constraint in the lepton-neutrino system and take the smaller p_z from the two solutions. If there is no solution for p_z, we take the real part of the solution of the quadratic equation. Figure 11 shows the reconstructed pz of neutrino momentum vs the generator neutrino momentum using Technicolor signal sample ($m(\rho_T^{\pm})$ = 200, $m(\pi_T^0)$ = 115 GeV/c^2) and comparison of the reconstructed dijet(ρ_T) mass for both solution case. We use both solution types because it was reported $W^{\pm}+2$ jet mass is not different between them in previous analysis. Figure 12 shows the dijet mass, W + 2jets mass, Q value defined by $Q = m(\rho_T) - m(\pi_T) - m(W)$ and 2D dijet mass vs Q value plots for Technicolor signal sample ($m(\rho_T^{\pm})$ = 200, $m(\pi_T^0)$ = 115 GeV/c^2).

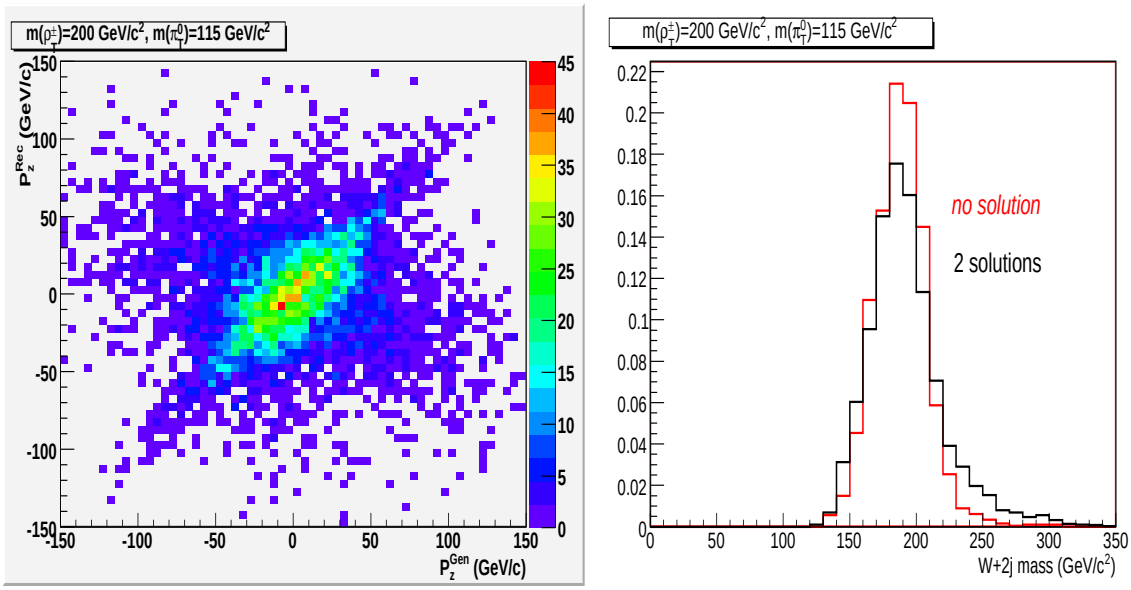

Figure 11: Left: The momentum of z component of reconstructed neutrino vs the momentum of z component of neutrino in generator level using nominal mass sample ($m(\rho_T^{\pm})$ = 200 GeV, $m(\pi_T^0)$ = 115 GeV). Right: The difference of W+2jet mass shapes between 2 solution and no solution case.

Figure 13-18 show the reconstructed dijet mass, $W^{\pm}$ + 2jet mass and Q value defined by $Q = m(\rho_T^{\pm}) - m(\pi_T^0) - m(W)$ for observed data, expected background and Technicolor signal($m(\rho_T^{\pm/0})$=200 GeV, $m(\pi_T^{0/\mp})$=115 GeV) for three tag categories. Q value and dijet mass are used to calculate 95% C.L. limit. According to these plots, observed data shape are

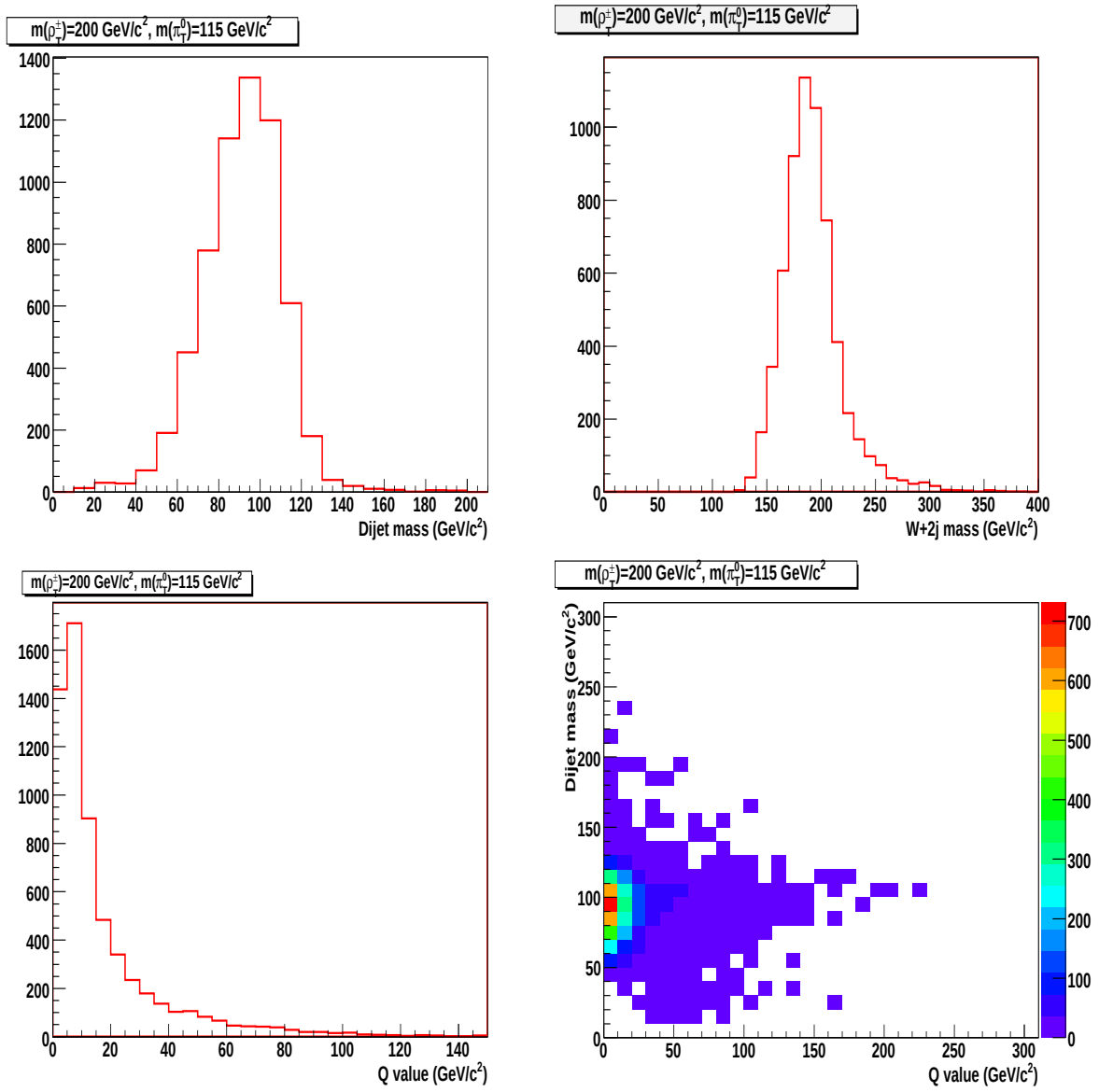

Figure 12: The reconstructed Technipi mass, Technirho mass, Q value and reconstructed Technipi mass vs Q value for pre-tagged events in nominal sample ($m(\rho_T^{\pm})$ = 200 GeV, $m(\pi_T^0)$ = 115 GeV)

consistent with expcted background shape within the uncertainty.

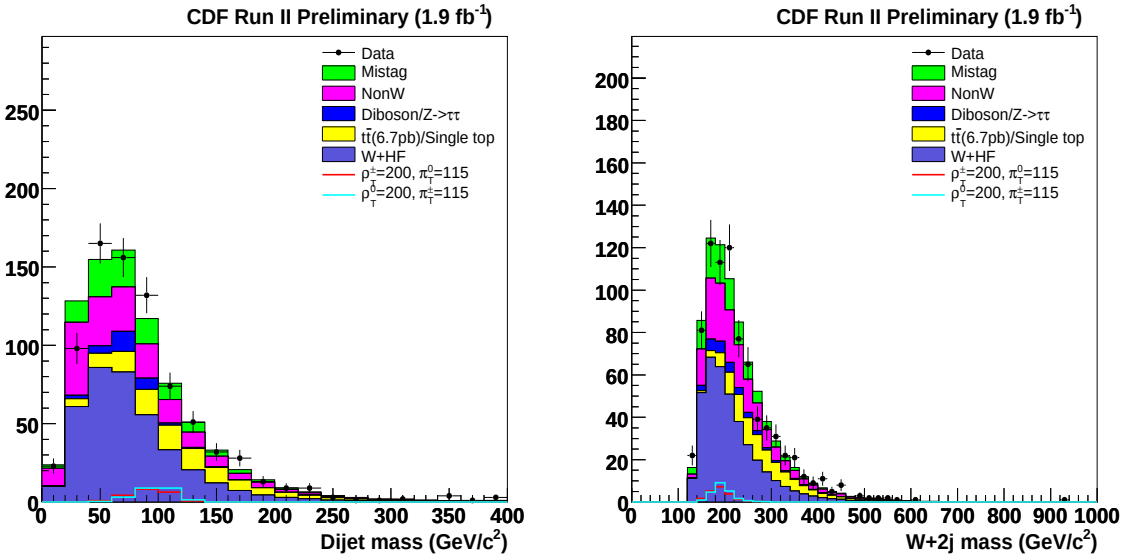

Figure 13: The reconstructed dijet mass and $W^{\pm}$ + 2jet mass distributions of expected background and observed data in exact 1 secVtx tag with NN tag.

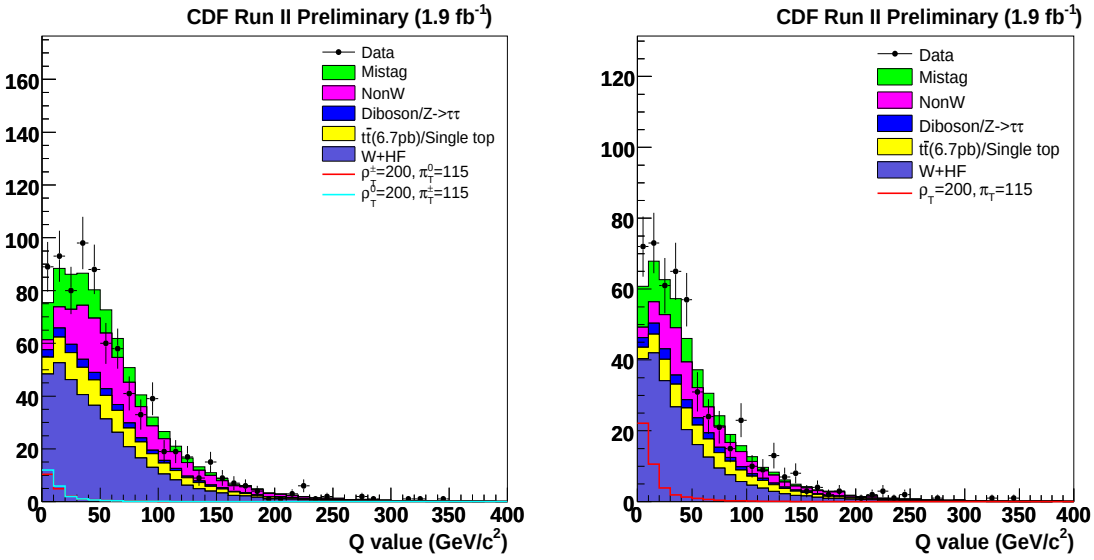

Figure 14: Left: The Q value distribution of expected background and observed data in exact 1 secVtx tag with NN tag. Right: The Q value distribution after dijet mass 2σ cut (m(ρ_T), m(π_T) = 200,115 GeV) are applied in exact 1 secVtx tag with NN tag.

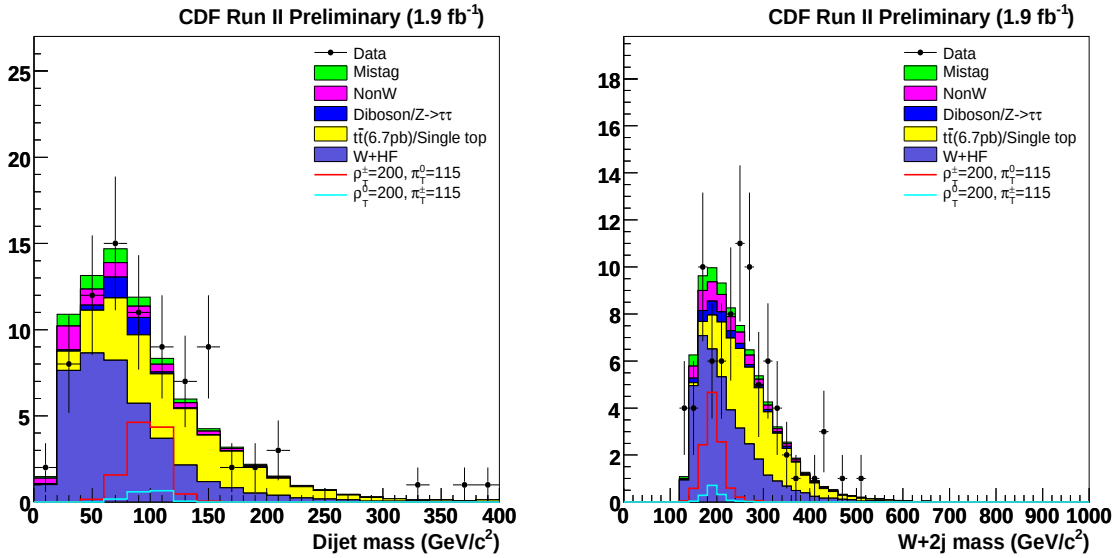

Figure 15: The reconstructed dijet mass and $W^{\pm}$ + 2jet mass distributions of expected background and observed data in ST+ST tag.

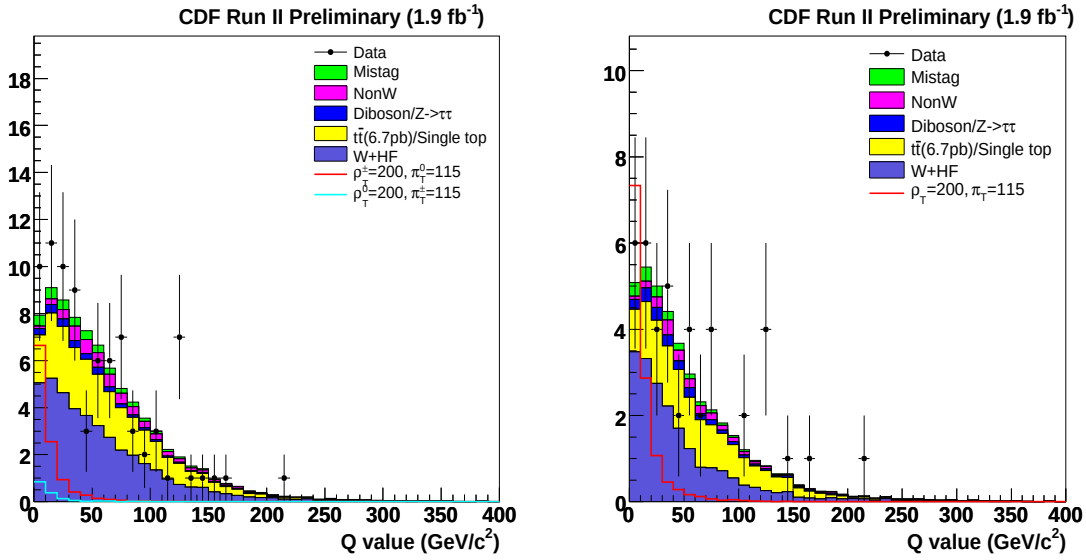

Figure 16: Left: The Q value distribution of expected background and observed data in ST+ST tag. Right: The Q value distribution after dijet mass 2σ cut (m(ρ_T), m(π_T) = 200,115 GeV) are applied in ST+ST tag.

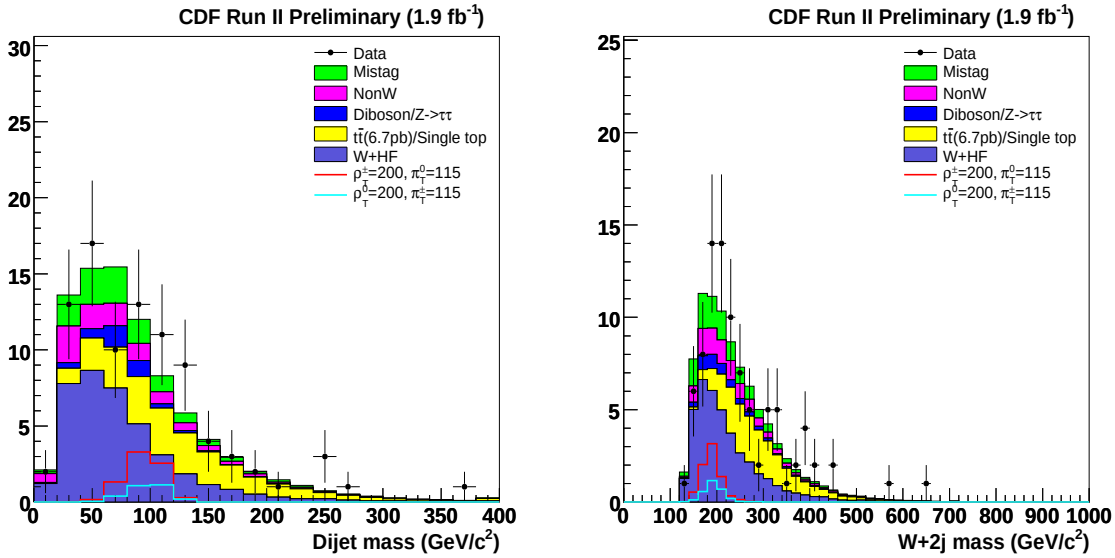

Figure 17: The reconstructed dijet mass and $W^{\pm}$ + 2jet mass distributions of expected background and observed data in ST+JP tag.

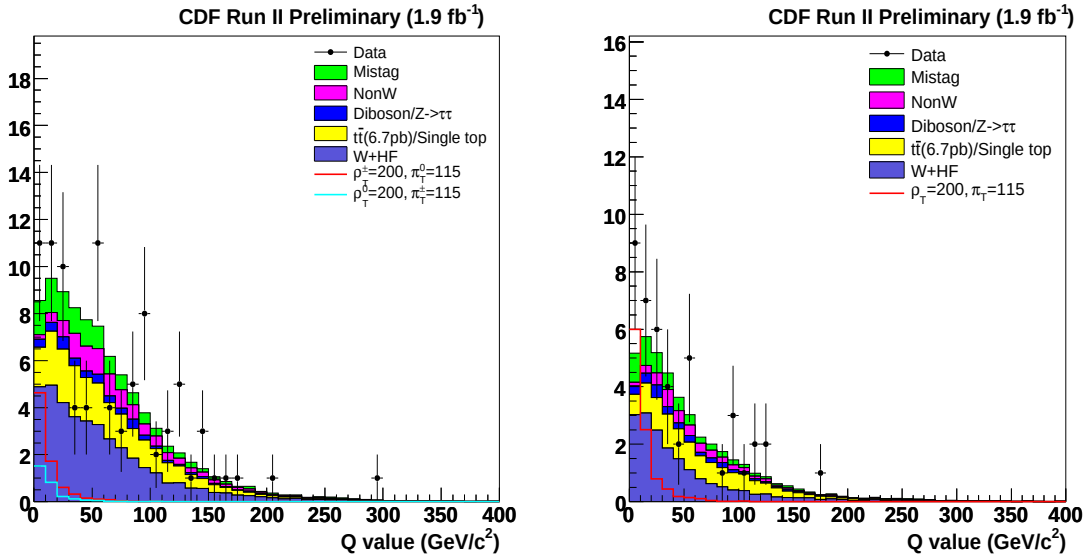

Figure 18: Left: The Q value distribution of expected background and observed data in ST+JP tag. Right: The Q value distribution after dijet mass 2σ cut (m(ρ_T), m(π_T) = 200,115 GeV) are applied in ST+JP tag.

8 Kinematic shape

We check the kinematics for each tagging category to make sure that the background compositions are well understood between data and Monte Carlo. The non-W shape is derived from the anti-electron. The W+jets shape is determined from Monte Carlo using ALPGEN_v2 and is normalized to the data after subtracting other backgrounds in pretag. The mistag shape is obtained from the data events before tagging, but weighted by the mistag matrix. The rest of the backgrounds, such as $t\bar{t}$, single top and diboson, are derived from Monte Carlo simulation with a top mass of 175 GeV/c^2. We add signal shape for each tagging category after scaling to able to see signal shape.

8.1 pretag

Figures 19-24 show the fundamental observed and expected shapes of lepton, Missing energy and two jets and correlation between these variables in the pretag sample in the W+2jet bin. As we mentioned, the background estimation is normalized to the number of events observed in the data. These plots show good agreement between the data and the background prediction.

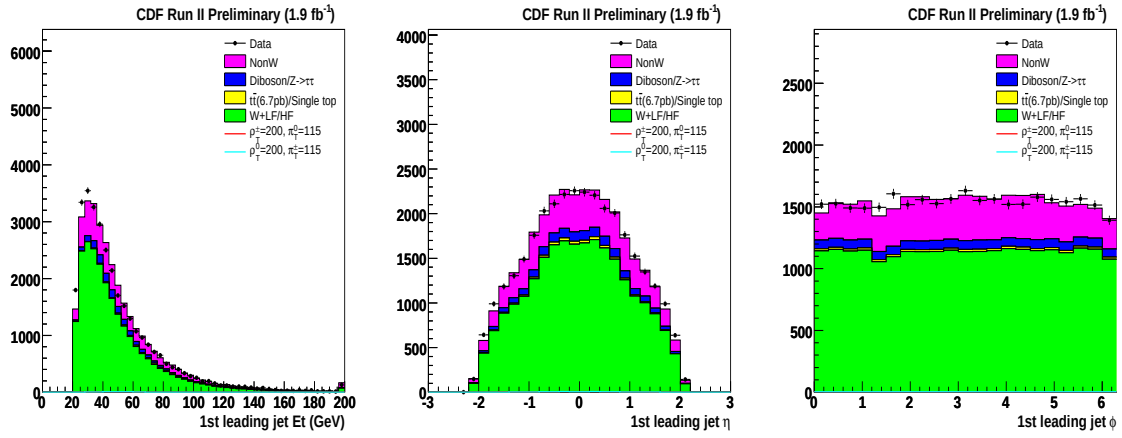

Figure 19: The first leading jet E_T, η and ϕ kinematic distributions in the pretag events. The W+jets background is normalized to the data after subtracting other backgrounds.

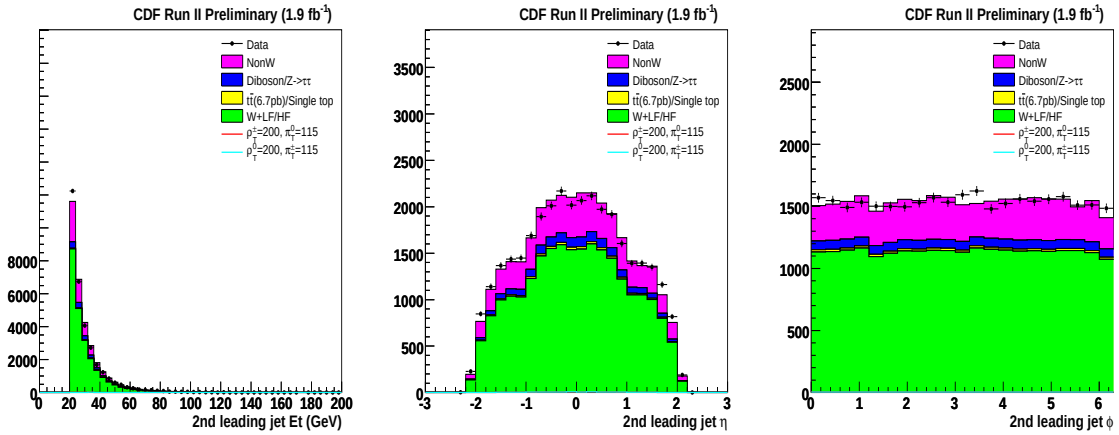

Figure 20: The second leading jet E_T, η and ϕ kinematic distributions in the pretag events. The W+jets background is normalized to the data after subtracting other backgrounds.

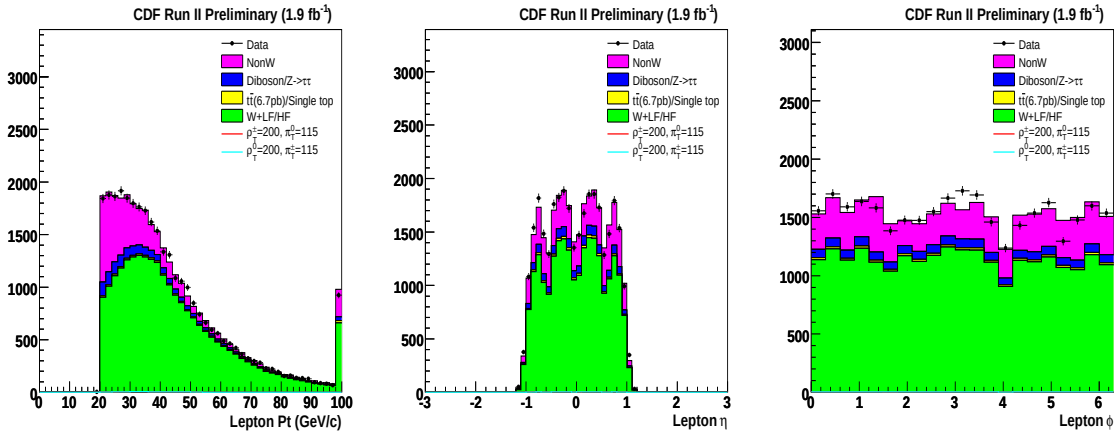

Figure 21: The lepton P_T, η and ϕ kinematic distributions in the pretag events. The W+jets background is normalized to the data after subtracting other backgrounds.

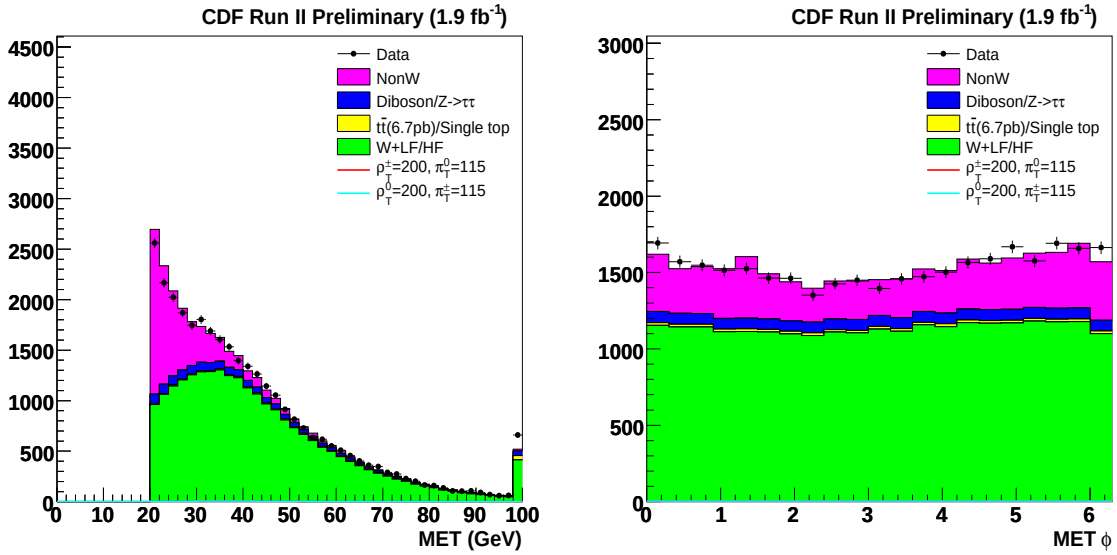

Figure 22: The $\not\!\!E_T$ and ϕ kinematic distributions in the pretag events. The W+jets background is normalized to the data after subtracting other backgrounds.

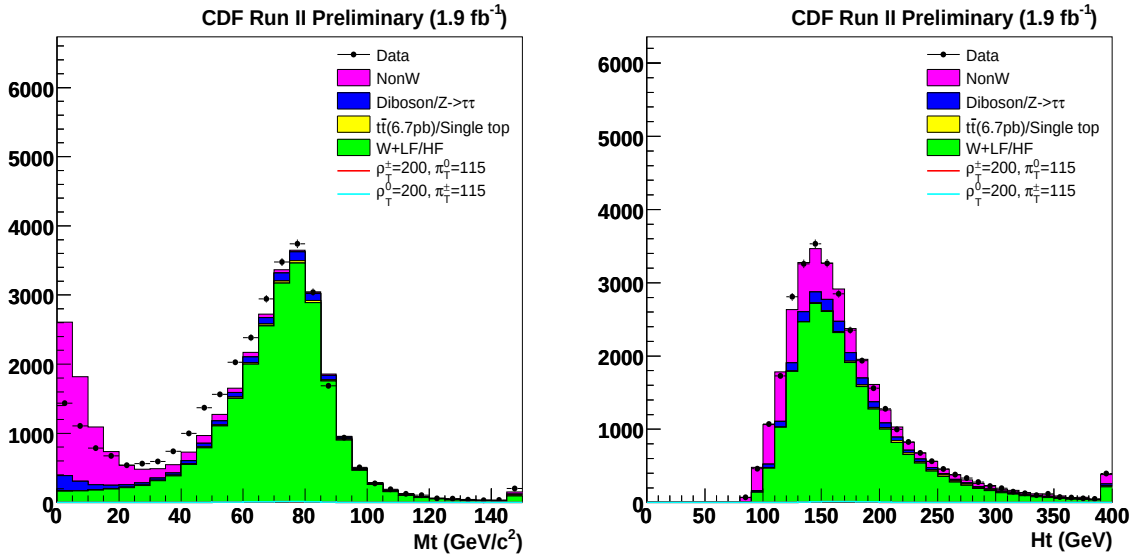

Figure 23: The reconstructed W transverse mass and Ht distributions in the pretag events. The W+jets background is normalized to the data after subtracting other backgrounds.

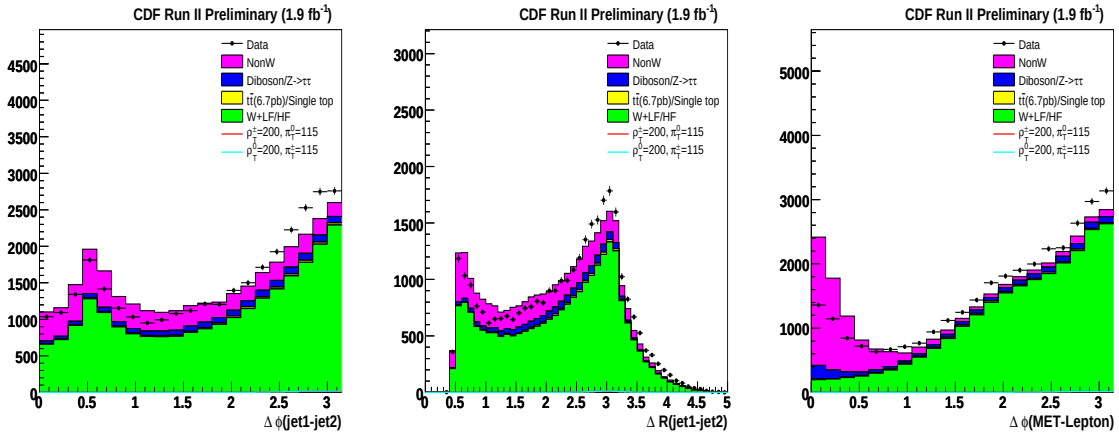

Figure 24: The observed and expected $\Delta\phi$ or ΔR between dijet and $\Delta\phi$ between $\not\!\!E_T$ and lepton in the pretag events. The W+jets background is normalized to the data after subtracting other backgrounds.

8.2 One SECVTX tag w/ NNtag

Figures 25-30 show the similar plots for the one SECVTX w/ NN tagged events in the W+2jet bin. The each backgrounds are normalized according to their Method 2 estimations.

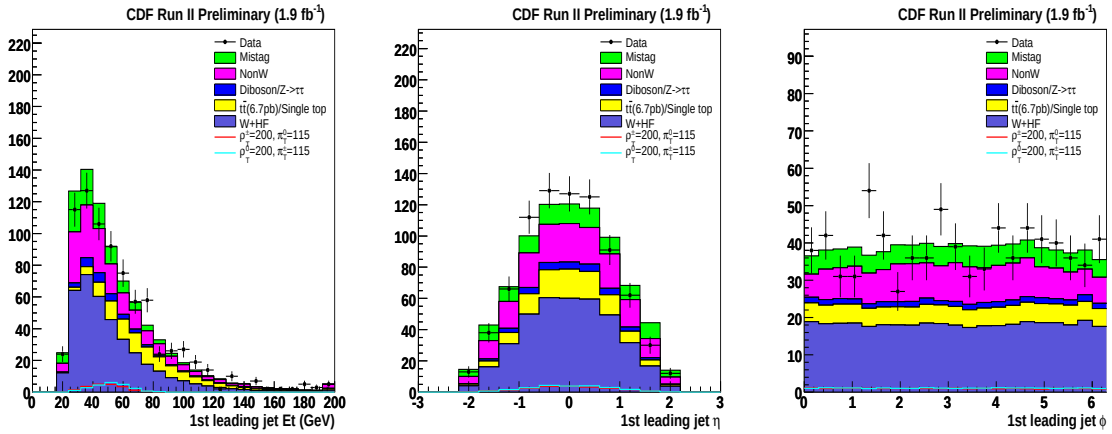

Figure 25: The first leading jet E_T, η and ϕ kinematic distributions in the one SECVTX w/ NN tagged events.

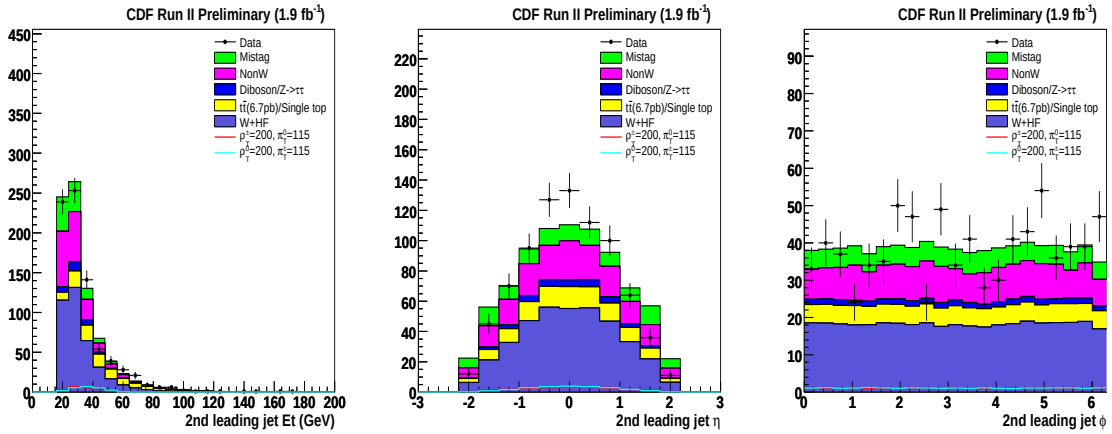

Figure 26: The second leading jet E_T, η and ϕ kinematic distributions in the one SECVTX w/ NN tagged events.

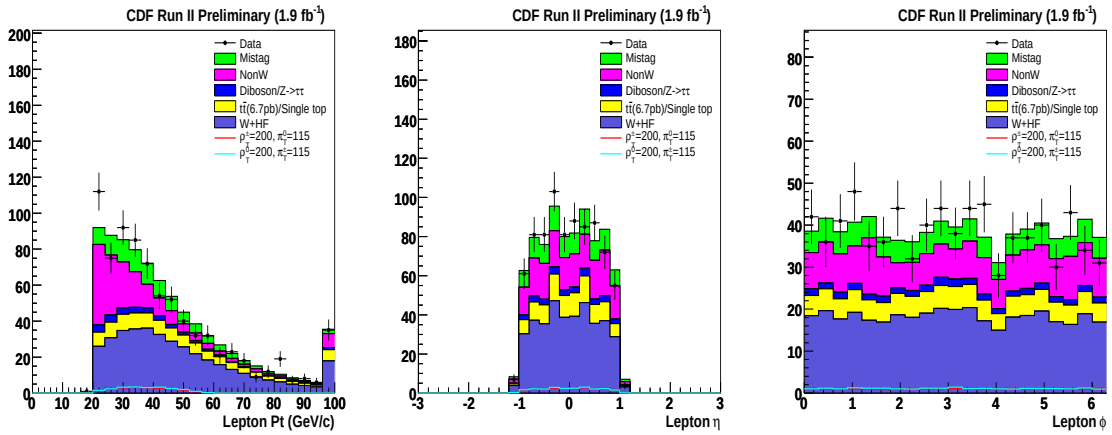

Figure 27: The lepton P_T, η and ϕ kinematic distributions in the one SECVTX w/ NN tagged events.

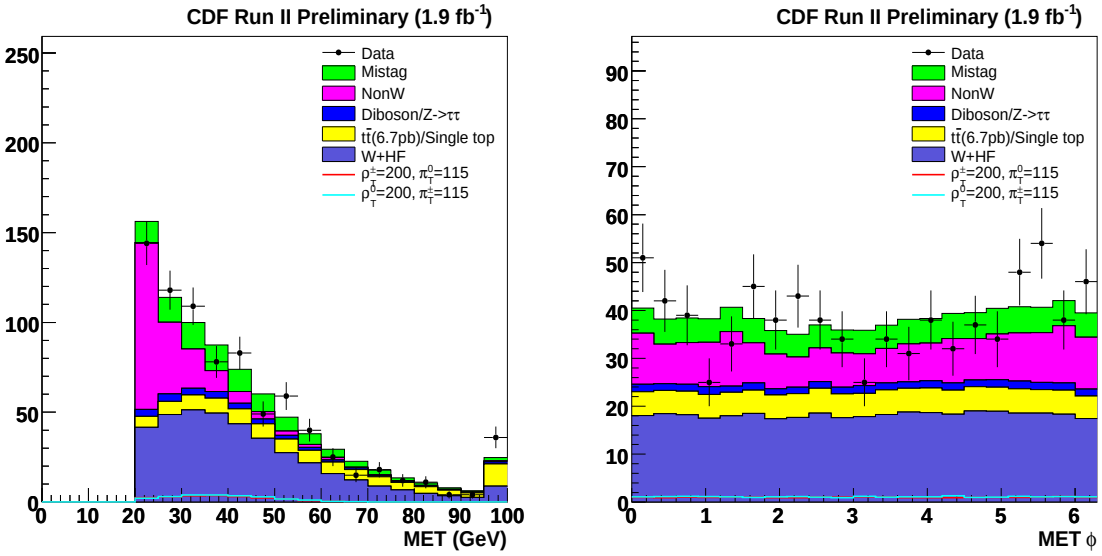

Figure 28: The $\not\!\!E_T$ and ϕ kinematic distributions in the one SECVTX w/ NN tagged events.

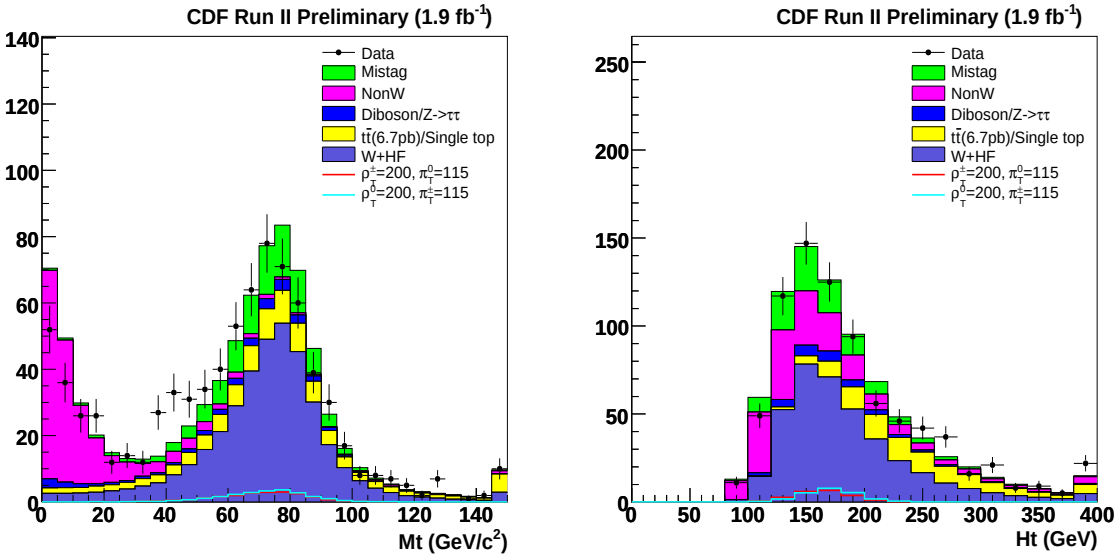

Figure 29: The reconstructed W transverse mass and Ht distributions in the one SECVTX w/ NN tagged events.

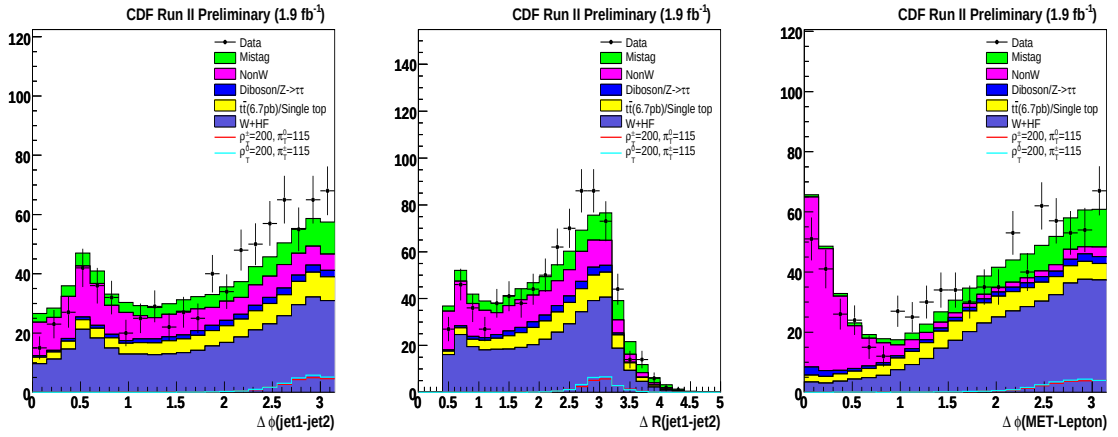

Figure 30: The observed and expected $\Delta\phi$ or ΔR between dijet and $\Delta\phi$ between $\not\!\!E_T$ and lepton in the one SECVTX w/ NN tagged events.

8.3 Double SECVTX tag

Figures 31-36 show the similar plots for the double SECVTX tagged events in the W+2jet bin. The each backgrounds are normalized according to their Method 2 estimations.

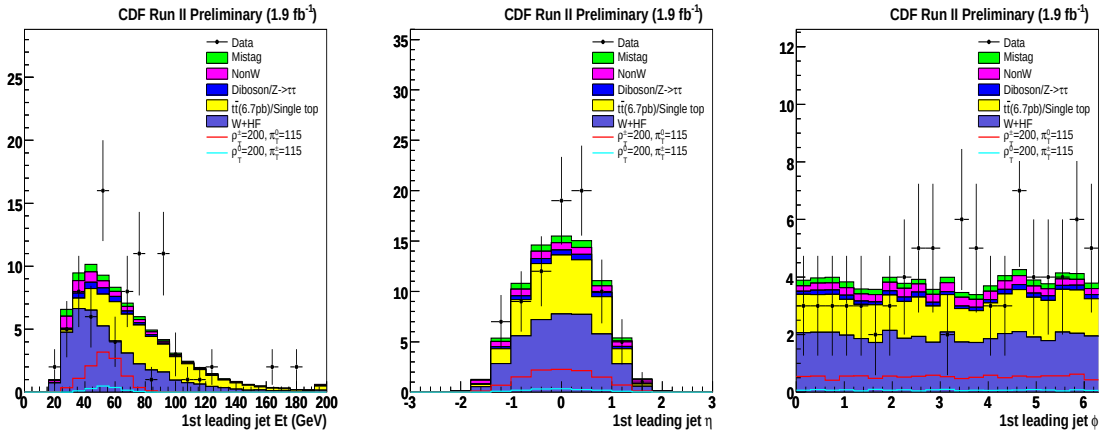

Figure 31: The first leading jet E_T, η and ϕ kinematic distributions in the double SECVTX tagged events.

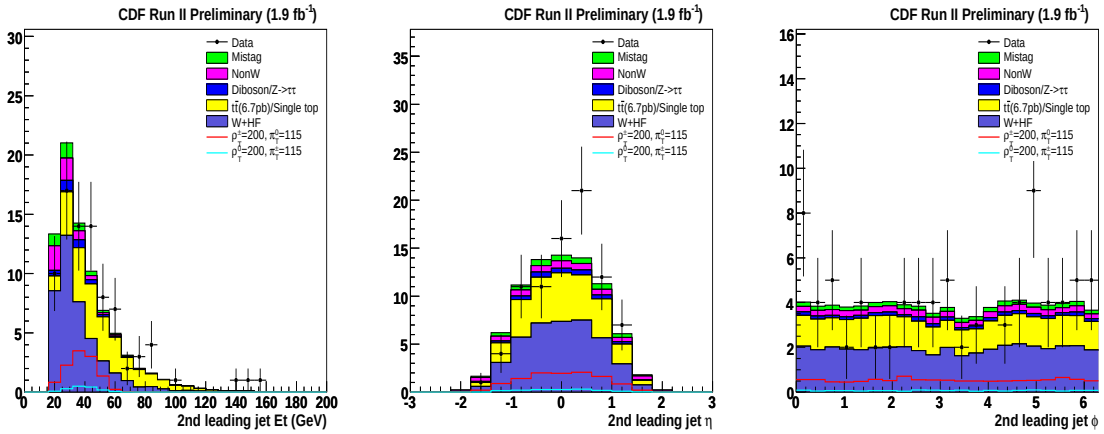

Figure 32: The second leading jet E_T, η and ϕ kinematic distributions in the double SECVTX tagged events.

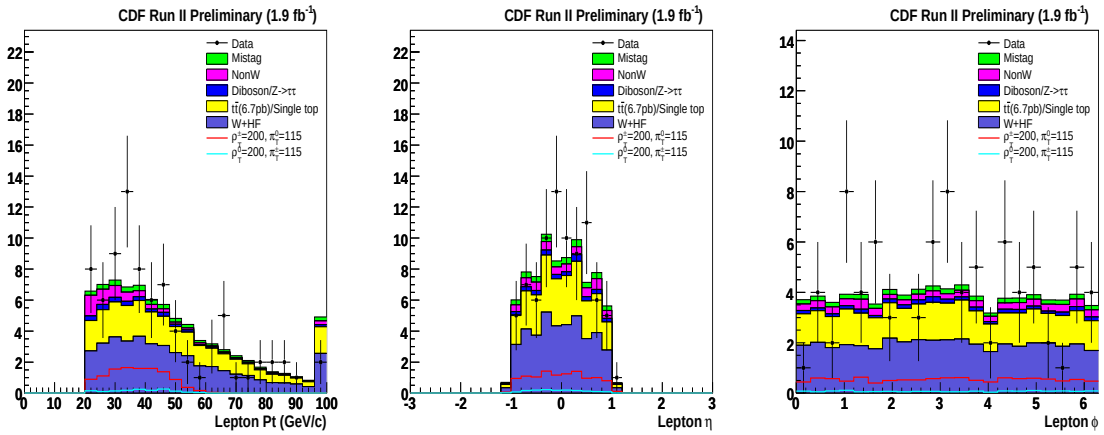

Figure 33: The lepton P_T, η and ϕ kinematic distributions in the double SECVTX tagged events.

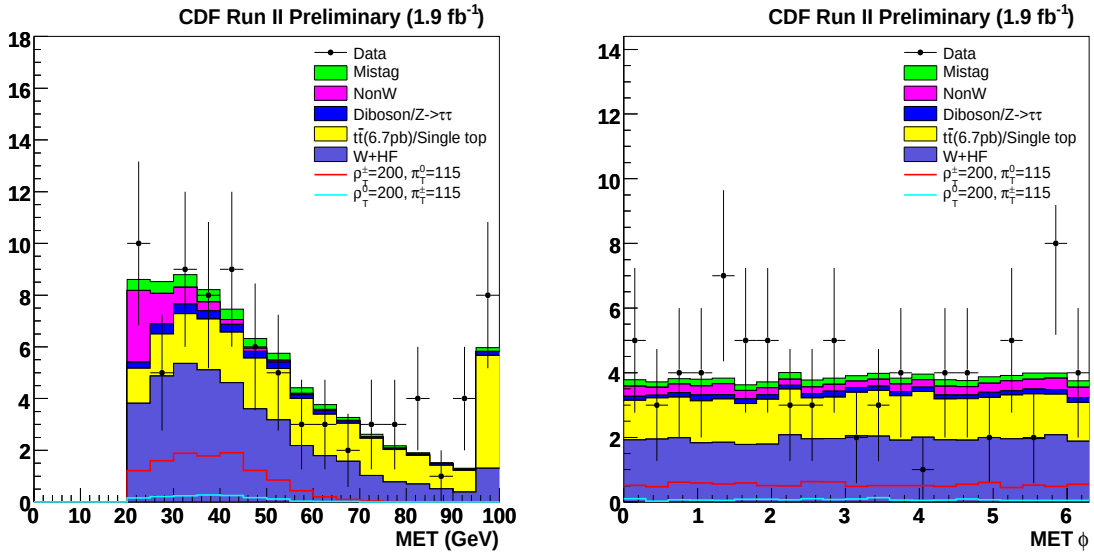

Figure 34: The $\not\!\!E_T$ and ϕ kinematic distributions in the double SECVTX tagged events.

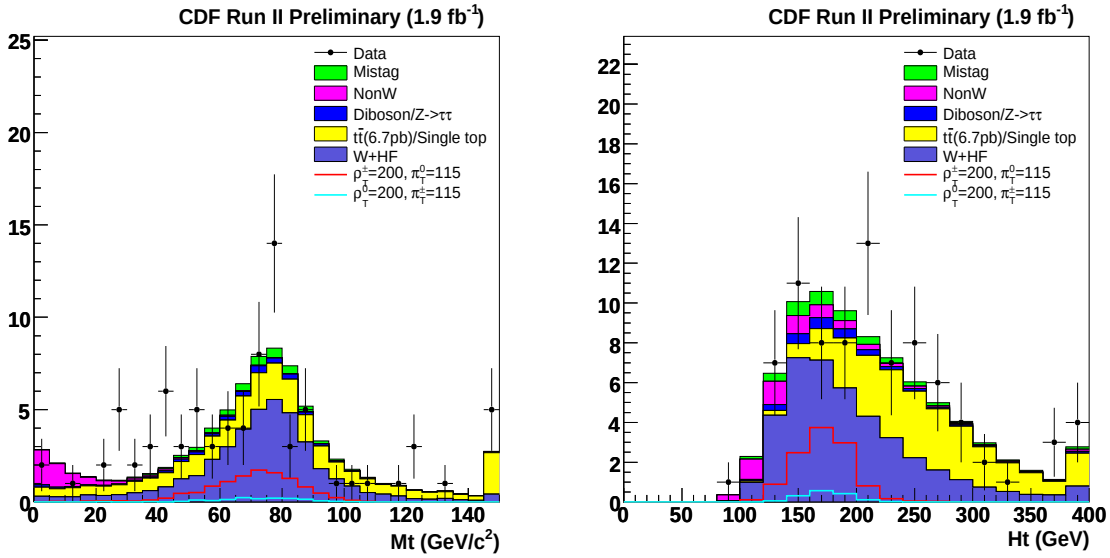

Figure 35: The reconstructed W transverse mass and Ht distributions in the double SECVTX tagged events.

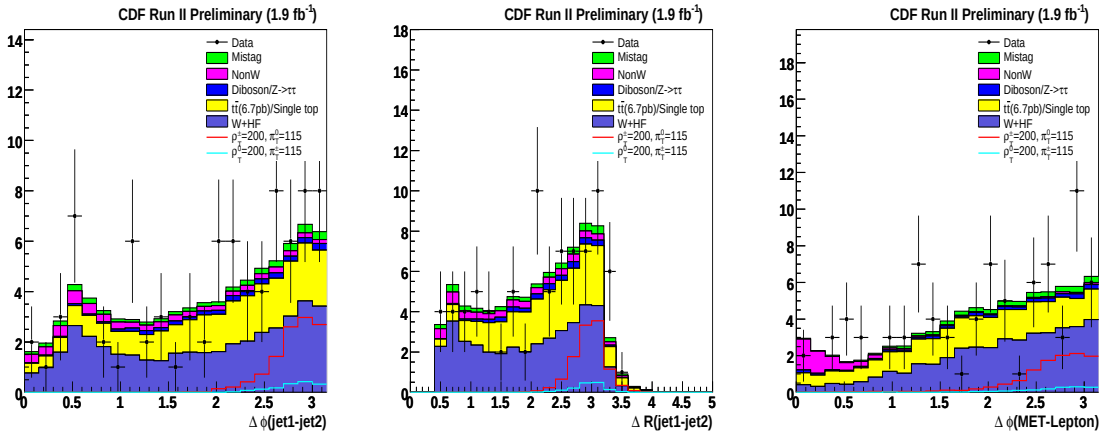

Figure 36: The observed and expected $\Delta\phi$ or ΔR between dijet and $\Delta\phi$ between $\not\!\!E_T$ and lepton in the double SECVTX tagged events.

8.4 One SECVTX tag and One jet probability tag

Figures 37-42 show the similar plots for the one SECVTX and one jet probability tagged events in the W+2jet bin. The each backgrounds are normalized according to their Method 2 estimations.

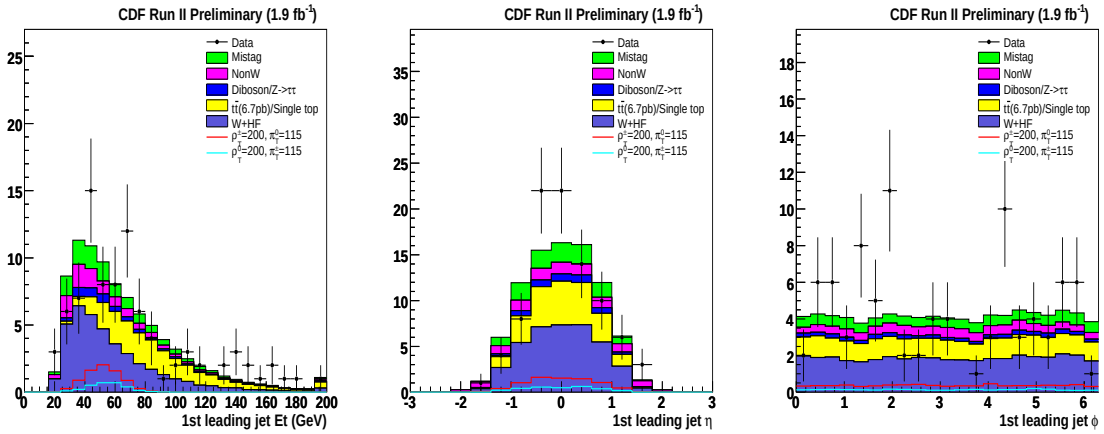

Figure 37: The first leading jet E_T, η and ϕ kinematic distributions in the one SECVTX + one jet probability tag events.

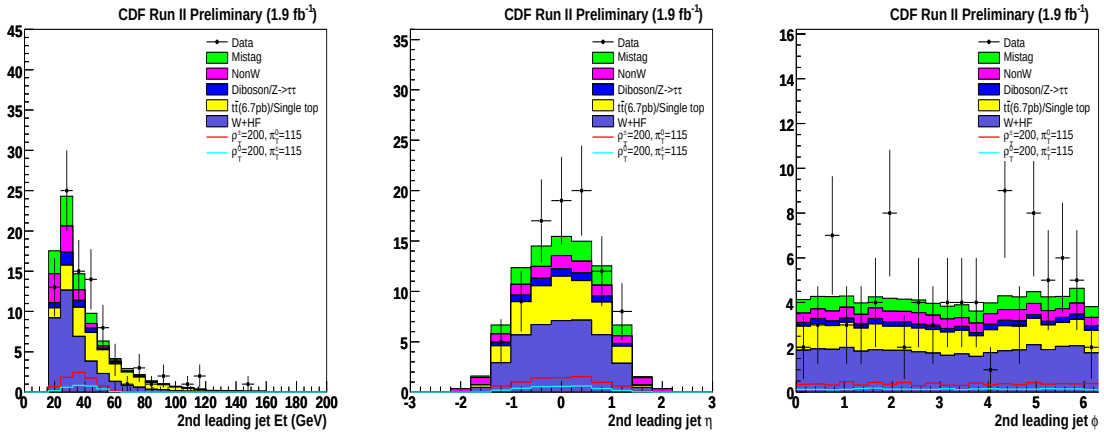

Figure 38: The second leading jet E_T, η and ϕ kinematic distributions in the one SECVTX + one jet probability tag events.

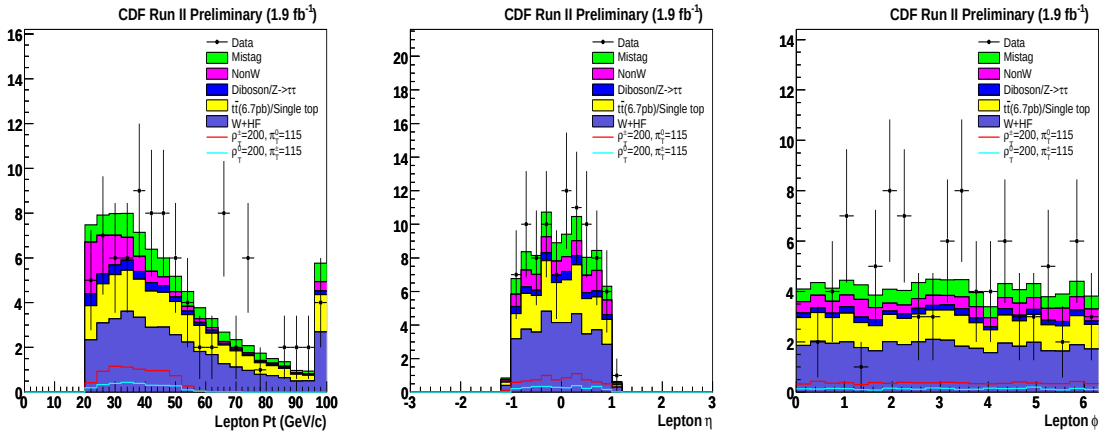

Figure 39: The lepton P_T, η and ϕ kinematic distributions in the one SECVTX + one jet probability tag events.

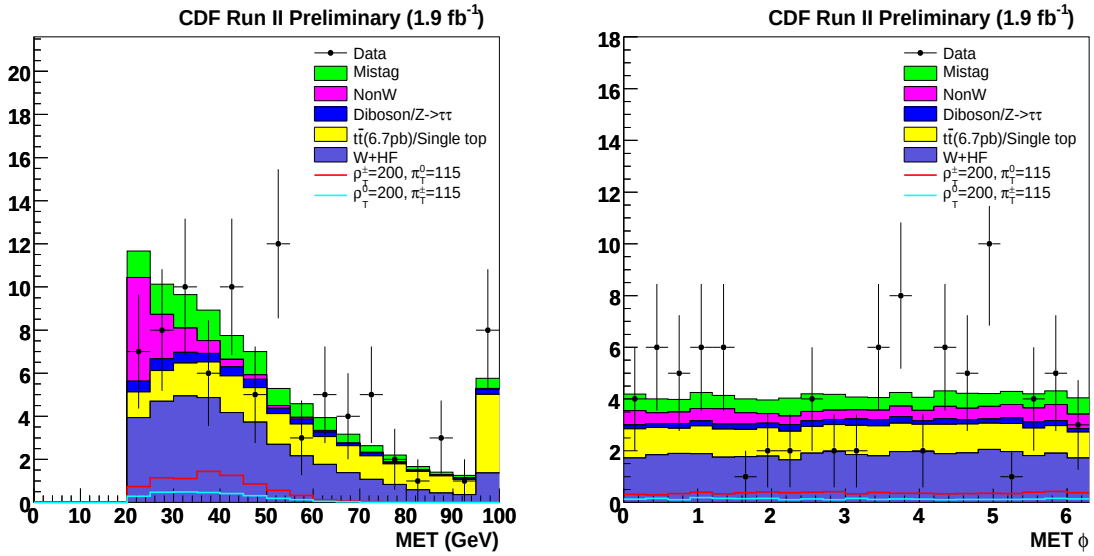

Figure 40: The $\not\!\!E_T$ and ϕ kinematic distributions in the one SECVTX + one jet probability tag events.

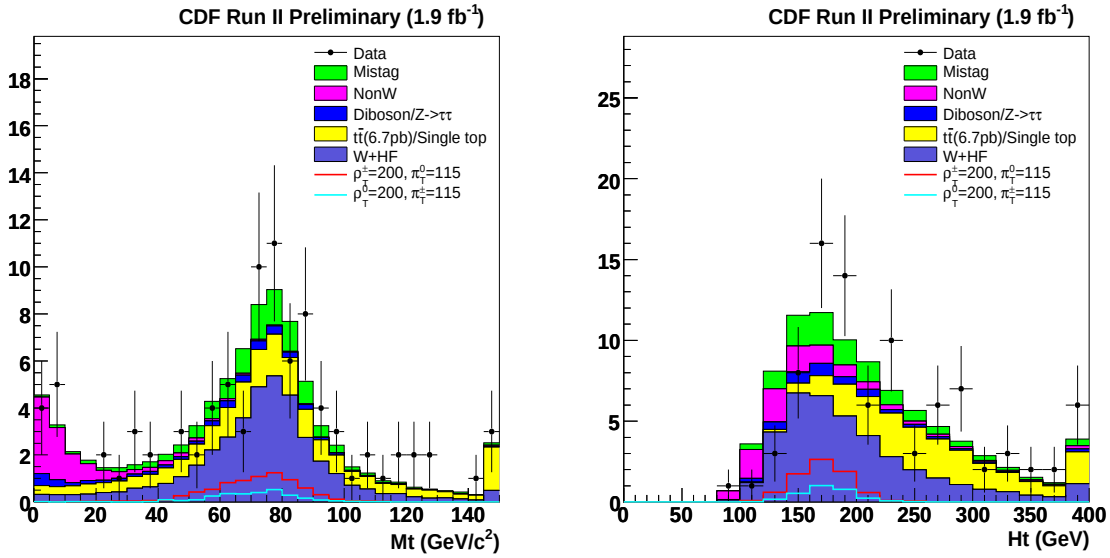

Figure 41: The reconstructed W transverse mass and Ht distributions in the one SECVTX + one jet probability tag events.

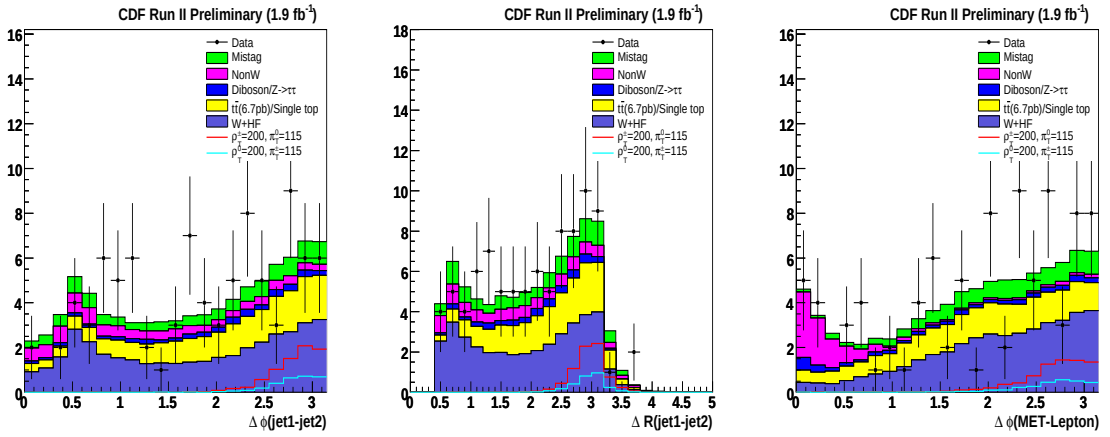

Figure 42: The observed and expected $\Delta\phi$ or ΔR between dijet and $\Delta\phi$ between $\not\!\!E_T$ and lepton in the one SECVTX + one jet probability tag events.

9 95% C.L. upper limit

We set an upper limit on the production cross section times branching ratio of $p\bar{p} \to \rho_T^{\pm/0} \to W^{\pm}\pi_T^{0/\mp}$ as a function of $m(\rho_T^{\pm/0})$ and $m(\pi_T^{0/\mp})$ by using the number of events in the $W^{\pm}+2$ jets sample since there are no mass peaks observed from $\rho_T^{\pm/0}$ and $\pi_T^{0/\mp}$. We assume the $W^{\pm}+2$ jets and dijet mass distributions in the data to consist of QCD (mistags, $W^{\pm}+b\bar{b}$, $W^{\pm}+c\bar{c}$, $W^{\pm}+c$, Z+jets and diboson), TOP ($t\bar{t}$ and single top) and $\rho_T^{\pm/0} \to W^{\pm}\pi_T^{0/\mp}$ events. A 2-dimensional binned maximum likelihood technique is used to obtain the limit on the cross section of signal process as in previous analysis. Figure [43-51] show the correlation between the Q value and the dijet mass for the each tag category for background and signal. The expected number of events (μ_{ij}) in each mass bin is

$$\mu_{ij} = f_{ij}^{QCD} \cdot N^{QCD} + f_{ij}^{TOP} \cdot N^{TOP} + f_{ij}^{\rho_T^{\pm/0} \to W^{\pm}\pi_T^{0/\mp}} \cdot (\varepsilon \cdot \mathcal{L} \cdot \sigma_{\rho_T^{\pm/0} \to W^{\pm}\pi_T^{0/\mp}}),$$

where f_{ij}^{QCD}, f_{ij}^{TOP} and $f_i^{\rho_T^{\pm/0} \to W^{\pm}\pi_T^{0/\mp}}$ are the expected fraction of events in a given mass bin predicted by Monte Carlo. N^{QCD}, N^{TOP}, ε, $\mathcal{L}$ and $\sigma_{\rho_T^{\pm/0} \to W^{\pm}\pi_T^{0/\mp}}$ are the expected number of QCD and TOP events, the detection efficiency, the luminosity and the unknown $\rho_T^{\pm/0} \to W^{\pm}\pi_T^{0/\mp}$ cross section respectively. In pseudo-experiment, to make the pseudo-data, we fluctuate the number of expected QCD and Top with Gaussian with the estimated total uncertainty independently, and also signal events with total systematic uncertainty. Then the corresponding likelihood is

$$L((\sigma \times BR)/(\sigma \times BR)_{theory}) = \iiint \prod_{i=bin} \prod_{j=bin} \frac{\mu_{ij}^{N_{ij}} \cdot e^{-\mu_{ij}}}{N_{ij}!} G(N_{QCD}, \sigma_{N_{QCD}}) G(N_{TOP}, \sigma_{N_{TOP}}) G(N_{Tc}, \sigma_{N_{Tc}}) dN_{QCD} dN_{TOP} dN_{Tc}, \quad (9)$$

We define the expected limit by taking the median value of the iterated pseudo-experiment. We try to calculate expected limit with three b-tag condition (1 SECVTX tagging with NN tag, double SECVTX tag and one SECVTX tag + one jet probability tag). The limit of "=1tag w/ NN tag & ST+ST tag & ST+JP combine" are obtained by combining the three likelihood of L(σ|1tag w/ NNtag), L(σ|STST) and L(σ|STJP) as

$$L(\sigma) = L(\sigma/\sigma_{theory}|1tagNNtag) \times L(\sigma/\sigma_{theory}|ST+ST) \times L(\sigma/\sigma_{theory}|ST+JP)$$

where the correlation between these three category events are taken into account like in WH analysis. The systematic uncertainties up to the pretag acceptance, luminosity uncertainty and uncertainty of b-tag scale factor are considered to be 100% correlated between the three selection criteria. Figure 52 show the expected limit normalized to theoretical cross section times branching ratio.

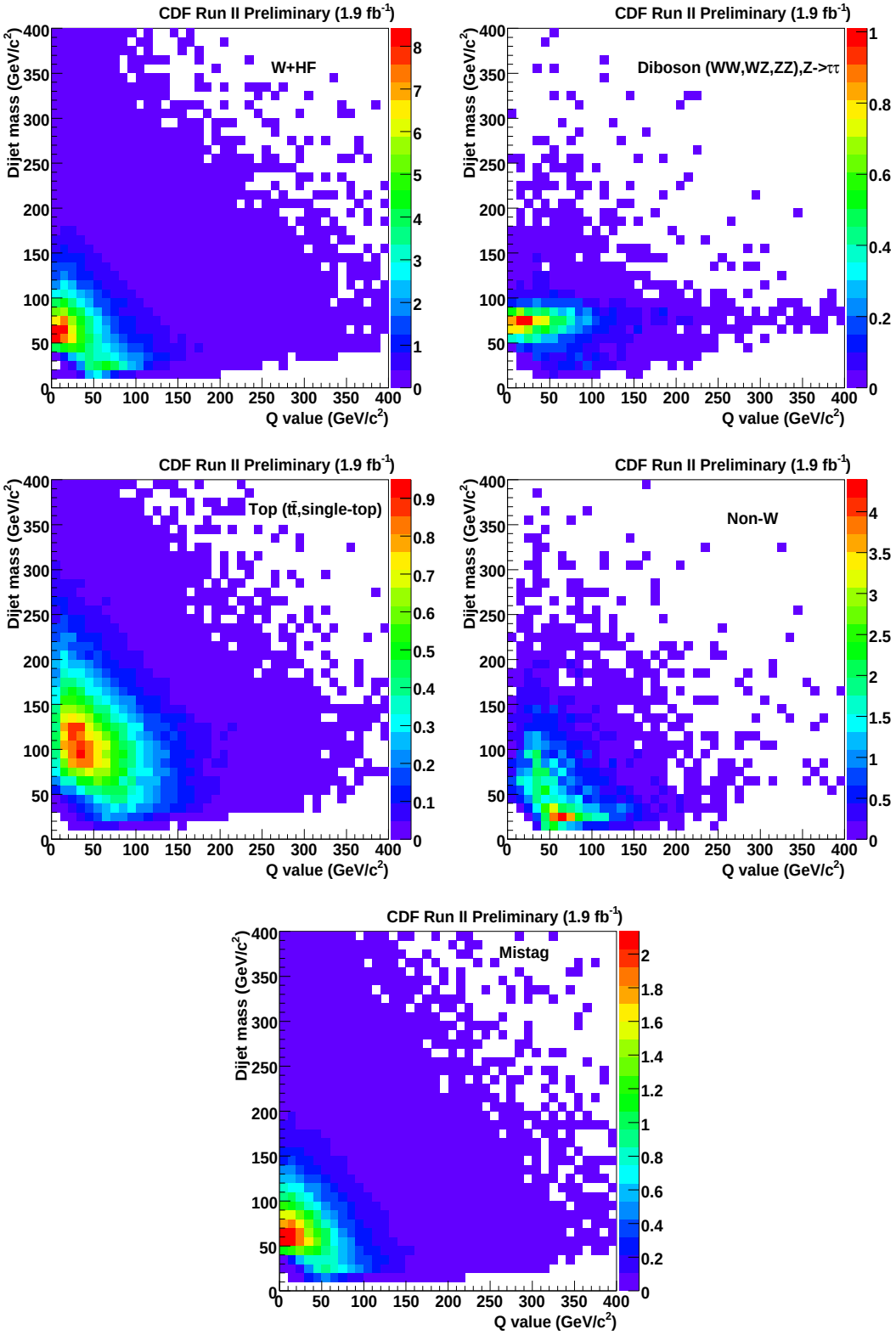

Figure 43: The reconstructed dijet mass vs Q value ($m(\rho_T^{\pm/0})$ - $m(\pi_T^{0/\mp})$ - m(W)) for each background components in exact 1 tag with NNtag.

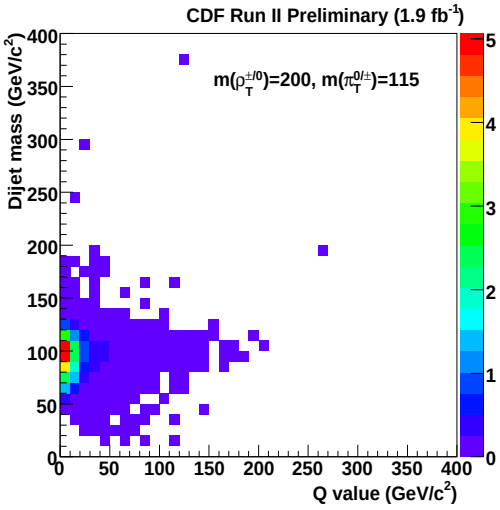

Figure 44: The reconstructed dijet mass vs Q value ($m(\rho_T^{\pm/0})$ - $m(\pi_T^{0/\mp})$ - m(W)) for signal nominal sample($m(\rho_T^{\pm/0})$=200,$m(\pi_T^{0/\mp})$=115 GeV) in exact 1 tag with NNtag. Both neutral and charged π_T is included as signal.

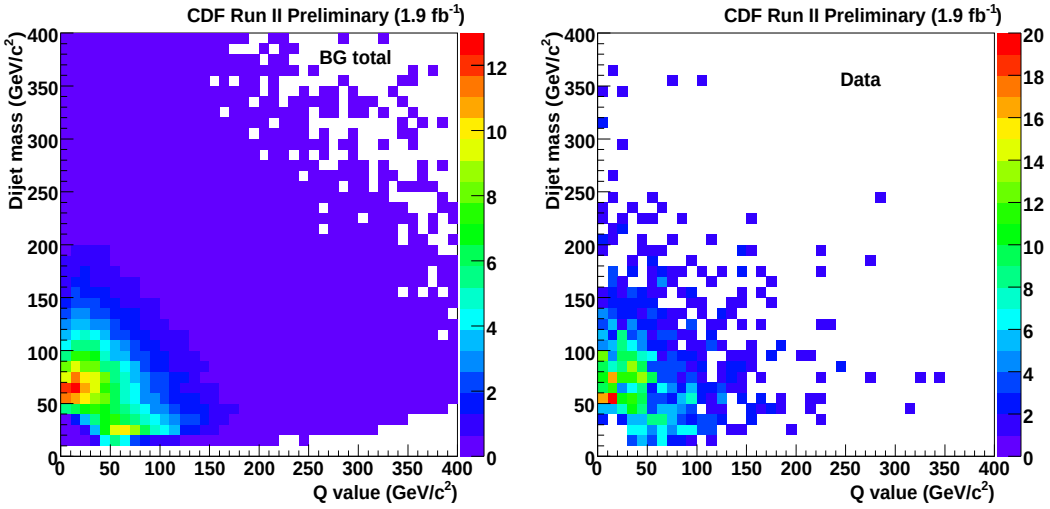

Figure 45: The reconstructed dijet mass vs Q value ($m(\rho_T^{\pm/0})$ - $m(\pi_T^{0/\mp})$ - m(W)) of total expected background and the data in exact 1 tag with NNtag.

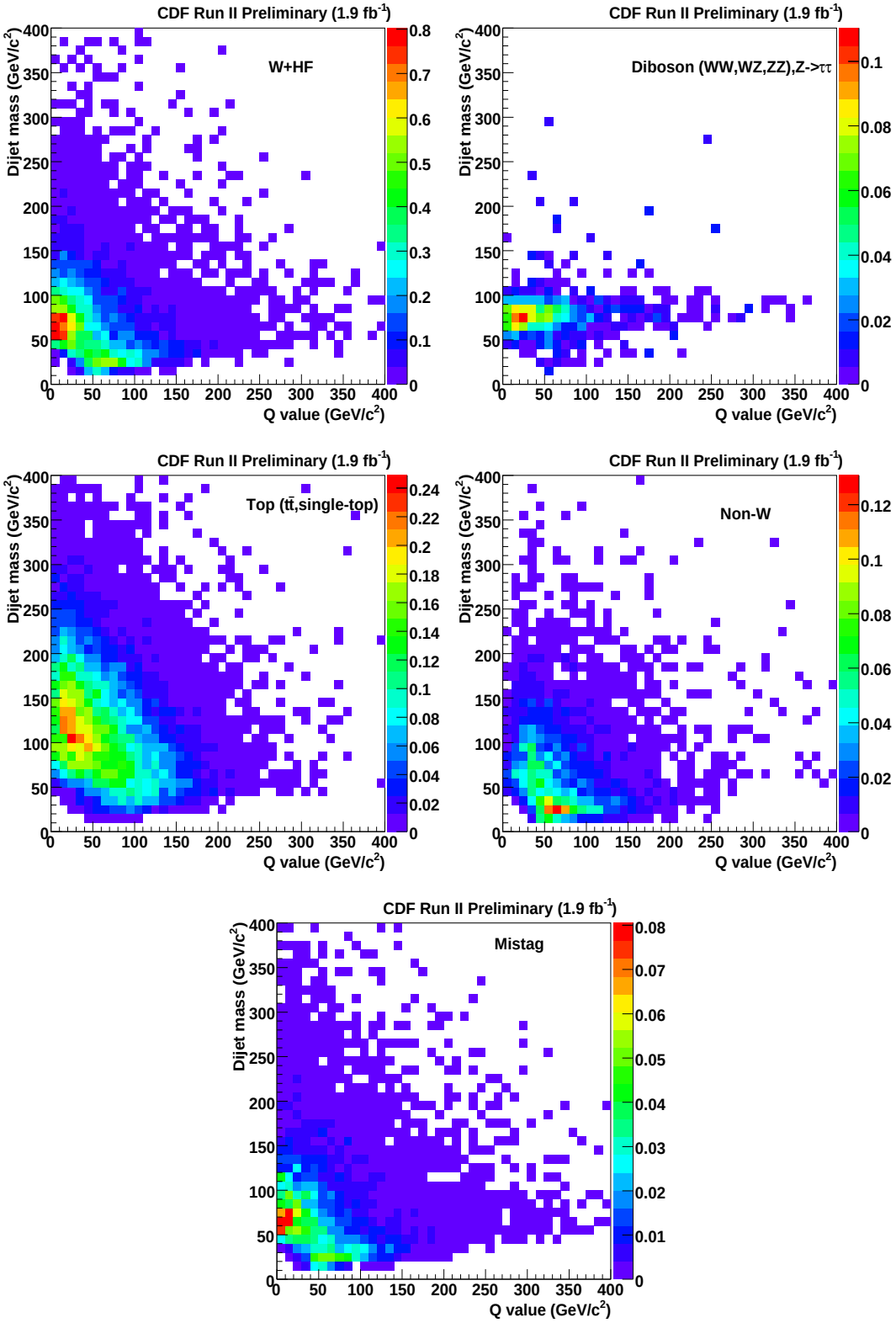

Figure 46: The reconstructed dijet mass vs Q value ($m(\rho_T^{\pm/0})$ - $m(\pi_T^{0/\mp})$ - m(W)) for each background components in ST+ST tag.

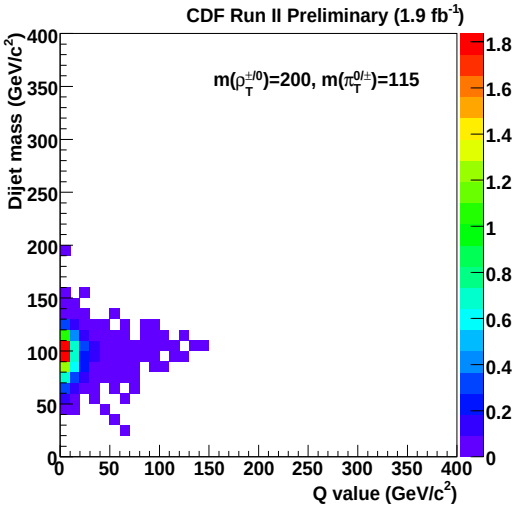

Figure 47: The reconstructed dijet mass vs Q value ($m(\rho_T^{\pm/0})$ - $m(\pi_T^{0/\mp})$ - m(W)) for signal nominal sample($m(\rho_T^{\pm/0})$=200,$m(\pi_T^{0/\mp})$=115 GeV) in ST+ST tag. Both neutral and charged π_T is included as signal.

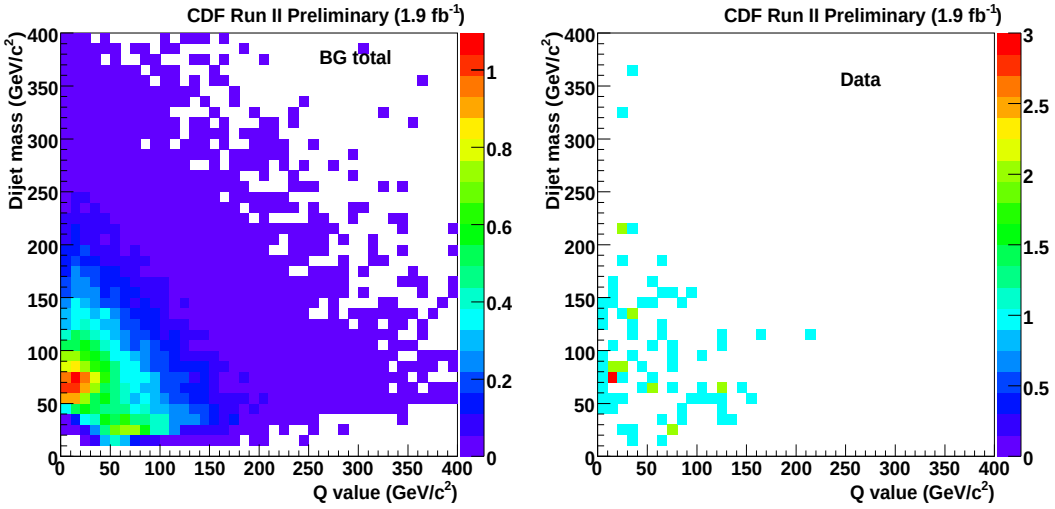

Figure 48: The reconstructed dijet mass vs Q value ($m(\rho_T^{\pm/0})$ - $m(\pi_T^{0/\mp})$ - m(W)) of total expected background and the data in ST+ST tag.

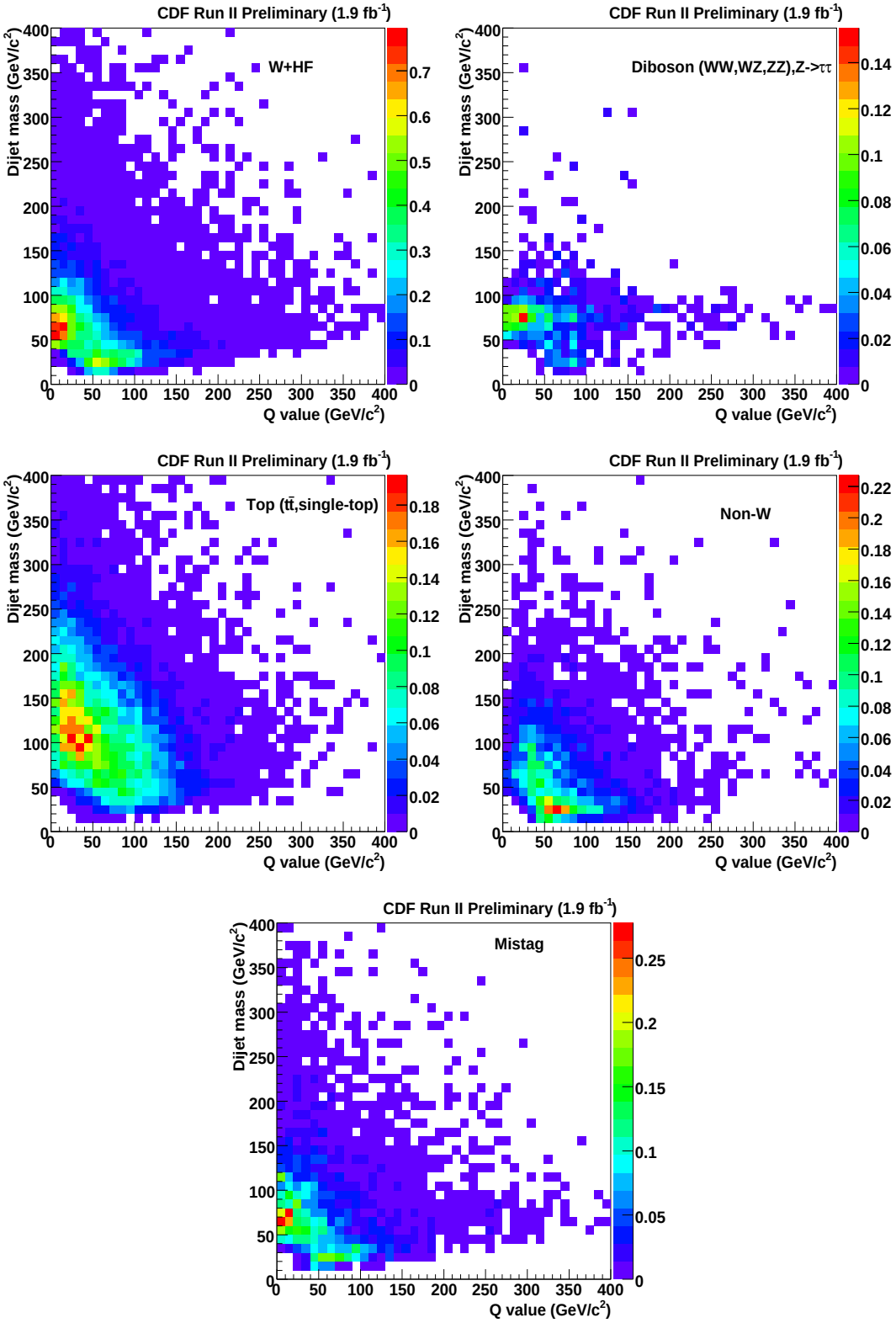

Figure 49: The reconstructed dijet mass vs Q value ($m(\rho_T^{\pm/0})$ - $m(\pi_T^{0/\mp})$ - m(W)) for each background components in ST+JP tag.

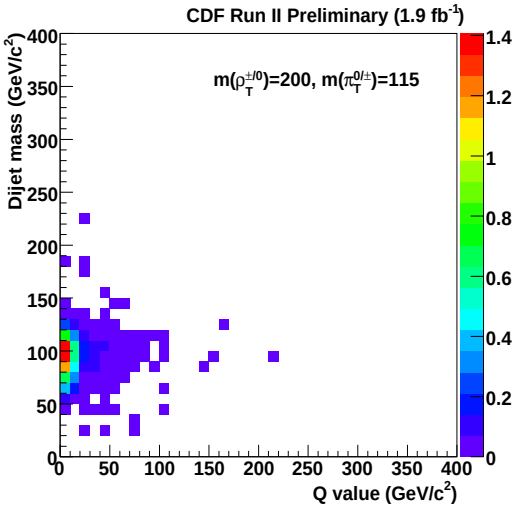

Figure 50: The reconstructed dijet mass vs Q value ($m(\rho_T^{\pm/0})$ - $m(\pi_T^{0/\mp})$ - m(W)) for signal nominal sample($m(\rho_T^{\pm/0})$=200,$m(\pi_T^{0/\mp})$=115 GeV) in ST+JP tag. Both neutral and charged π_T is included as signal.

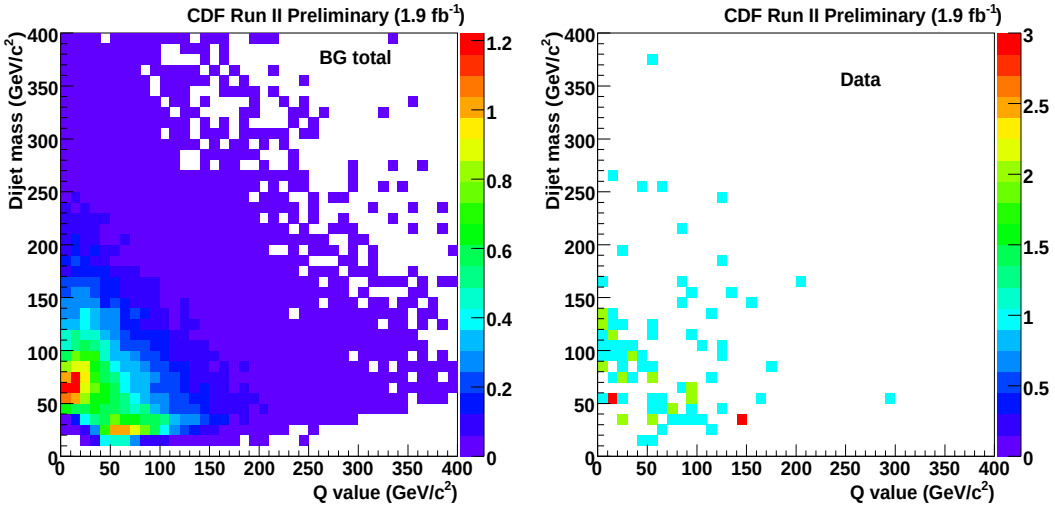

Figure 51: The reconstructed dijet mass vs Q value ($m(\rho_T^{\pm/0})$ - $m(\pi_T^{0/\mp})$ - m(W)) of total expected background and the data in ST+JP tag.

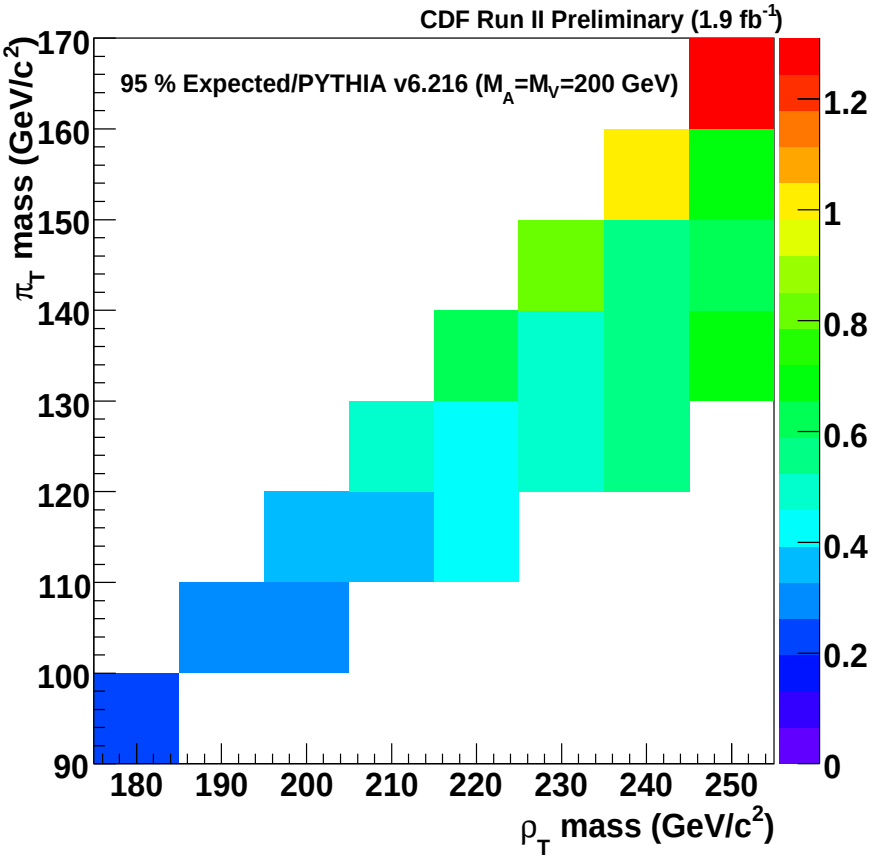

Figure 52: The expected limit of the each ρ_T, π_T mass point for combined three tag categories. Limits are normalized to theory cross section times branching ratio.

m(ρ_T)/m(π_T)	95GeV	105GeV	115GeV	125GeV	135GeV	145GeV	155GeV	165GeV
180 GeV	0.22	—	—	—	—	—	—	—
190 GeV	—	0.28	—	—	—	—	—	—
200 GeV	—	0.30	0.37	—	—	—	—	—
210 GeV	—	—	0.33	0.47	—	—	—	—
220 GeV	—	—	0.42	0.39	0.59	—	—	—
230 GeV	—	—	—	0.48	0.49	0.79	—	—
240 GeV	—	—	—	0.57	0.56	0.58	1.03	—
250 GeV	—	—	—	—	0.66	0.65	0.72	1.31

Table 14: This table shows combined expected upper limit using 2D dijet mass vs Q value fitting for each mass point. The values are upper limit normalized to theoretical expectation.

9.1 Observed limit

Finally, we set 95 % C.L upper limit on $\sigma(\rho_T^{\pm/0} \rightarrow W\pi_T^{0/\mp}) \times BR(\pi_T^{0/\mp} \rightarrow b\bar{q})$ using combined likelihood 1tag w/ NNtag, ST+ST tag and ST+JP tag. In figure 53, the observed limit is shown for the each mass point of $m(\rho_T^{\pm/0})$ and $m(\pi_T^{0\pm})$. In figure 54-55, the 95% C.L.upper limit results from one thousand pseudo-experiments and observed limit (red arrow) are shown.

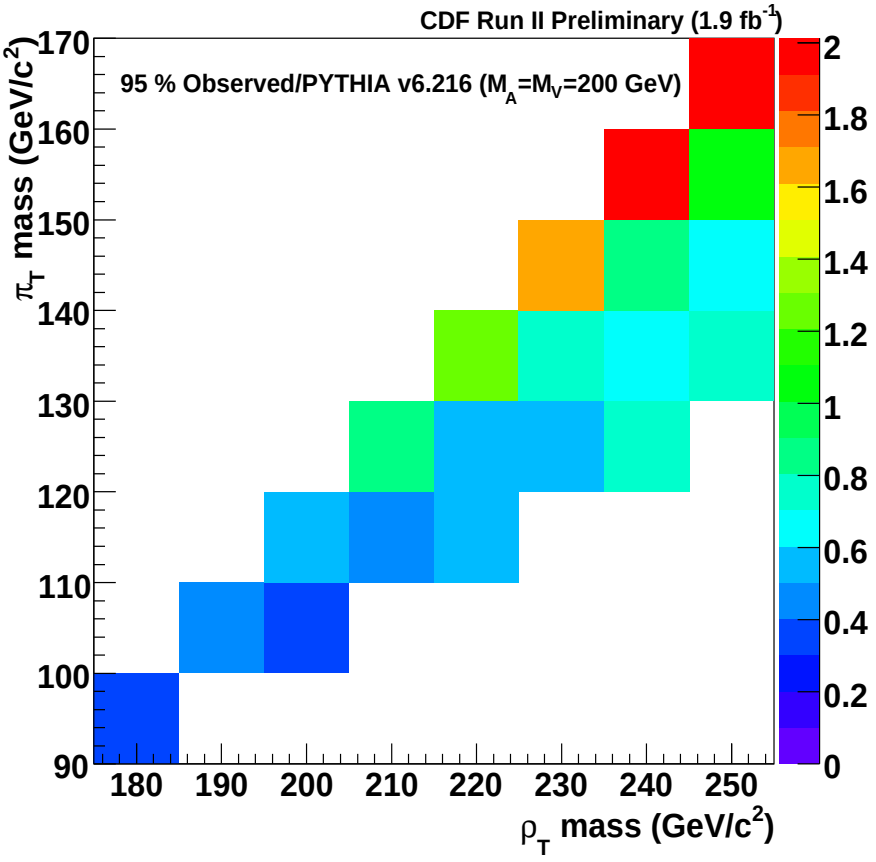

Figure 53: The observed limit of the each ρ_T, π_T mass point for combined three tag categories. Observed limits are normalized to theoretical cross section.

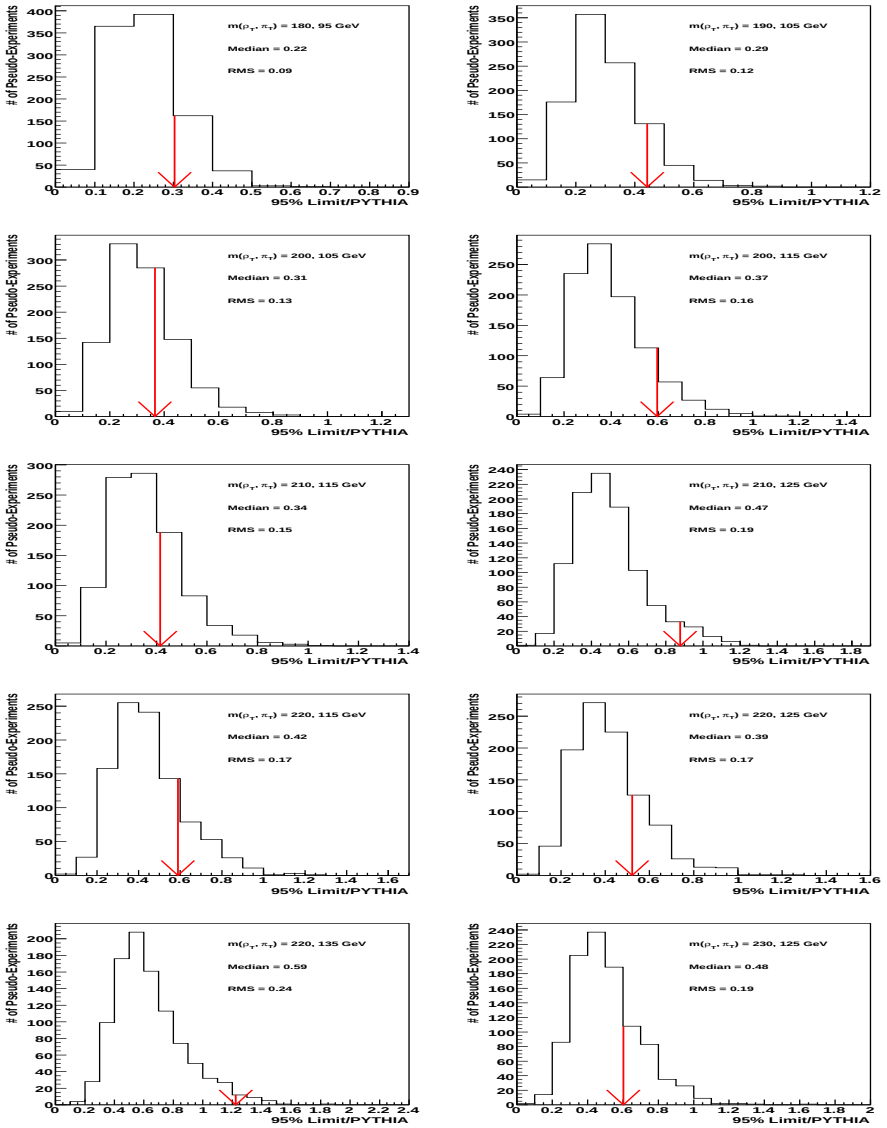

Figure 54: The results show 95% C.L. upper limit for each ρ_T, π_T mass point with one thousand pseudo experiments. The red arrows mean the observed upper limit.

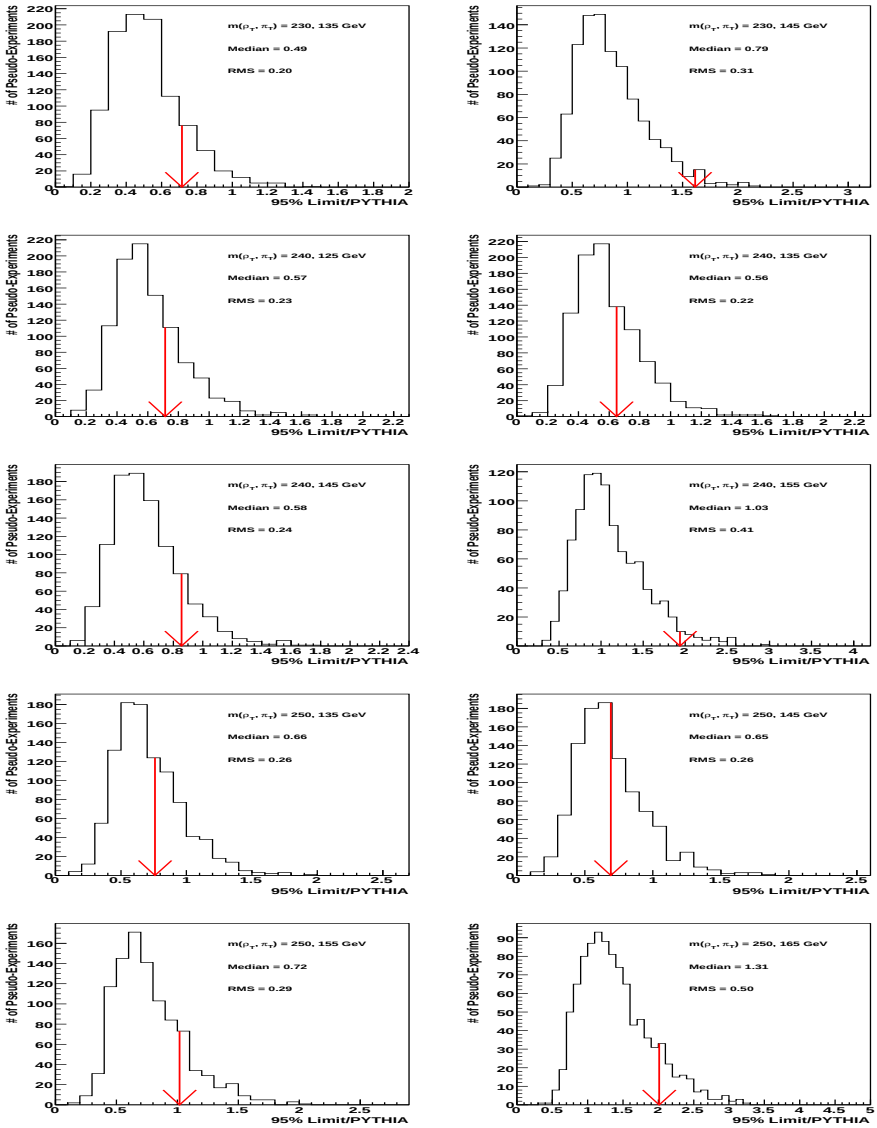

Figure 55: The results show 95% C.L. upper limit for each ρ_T, π_T mass point with one thousand pseudo experiments. The red arrows mean the observed upper limit.

m(ρ_T)/m(π_T)	95GeV	105GeV	115GeV	125GeV	135GeV	145GeV	155GeV	165GeV
180 GeV	0.30	—	—	—	—	—	—	—
190 GeV	—	0.44	—	—	—	—	—	—
200 GeV	—	0.37	0.59	—	—	—	—	—
210 GeV	—	—	0.42	0.88	—	—	—	—
220 GeV	—	—	0.59	0.52	1.22	—	—	—
230 GeV	—	—	—	0.60	0.72	1.61	—	—
240 GeV	—	—	—	0.71	0.65	0.86	1.94	—
250 GeV	—	—	—	—	0.76	0.69	1.02	2.01

Table 15: This table shows observed upper limit using 2D dijet mass vs Q value fit for each mass point. The values are upper limit normalized to theoretical expectation.

$m(\rho_T^{\pm/0})$	$m(\pi_T^{0/\mp})$ exclude region at 95% C.L.
180 GeV	$m(\pi_T^{0/\mp}) = 95$ GeV
190 GeV	$m(\pi_T^{0/\mp}) = 105$ GeV
200 GeV	$105 < m(\pi_T^{0/\mp}) < 115$ GeV
210 GeV	$115 < m(\pi_T^{0/\mp}) < 125$ GeV
220 GeV	$115 < m(\pi_T^{0/\mp}) < 125$ GeV
230 GeV	$125 < m(\pi_T^{0/\mp}) < 135$ GeV
240 GeV	$125 < m(\pi_T^{0/\mp}) < 145$ GeV
250 GeV	$135 < m(\pi_T^{0/\mp}) < 145$ GeV

Table 16: The excluded region at 95% C.L in the ($m(\rho_T)$-$m(\pi_T)$) plane for $\rho_T^{\pm/0} \rightarrow W\pi_T^{0/\mp} \rightarrow l\nu b\bar{q}$ production

10 Conclusions

We have presented a search for the Technicolor particles (Techni rho and Techni pion) using $\approx 1.9 fb^{-1}$ data. We find that the observed events agree with our background predictions. We set an upper limit on the production cross section times branching ratio as a function of techinicolor particle masses. We are able to exclude some Technicolor mass region with 95% C.L. The excluded region is listed in table16. Table 56-58 show the 95% C.L. expected and observed excluded region with 2-D plain.

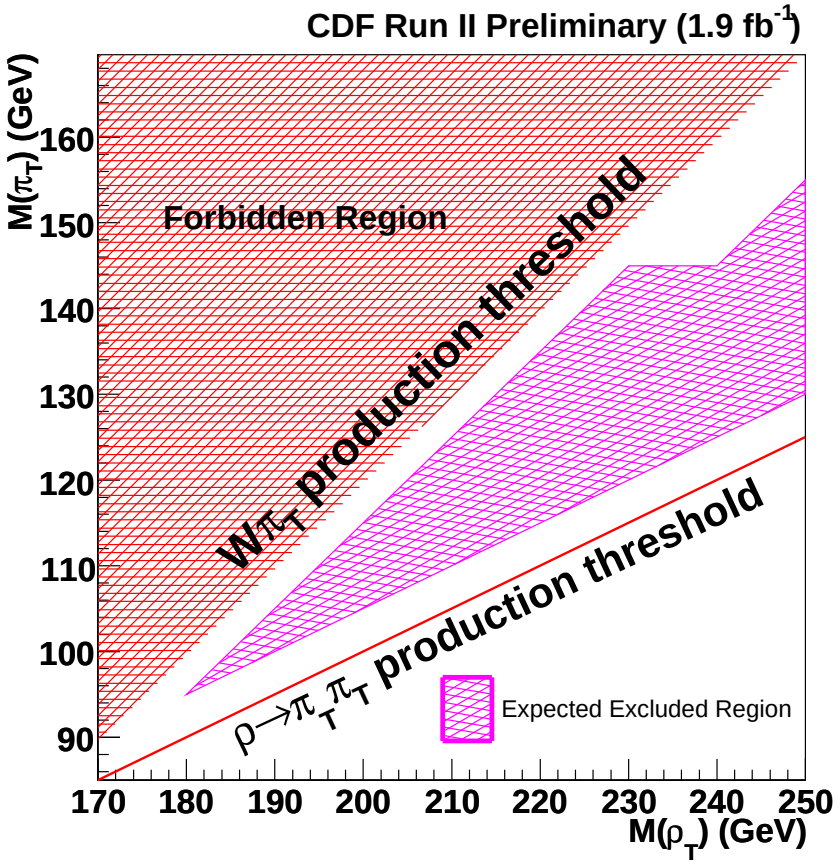

Figure 56: The expected excluded region at 95% C.L. in the ($m(\rho_T)$-$m(\pi_T)$) plane for $\rho_T^{\pm/0} \rightarrow W\pi_T^{0/\mp} \rightarrow l\nu b\bar{q}$ production. The magenta region means 95% C.L. expected excluded region. The red region is the forbidden region due to the Wπ_T production kinematical threshold. And the red line is the $\rho_T \rightarrow \pi_T\pi_T$ production threshold.

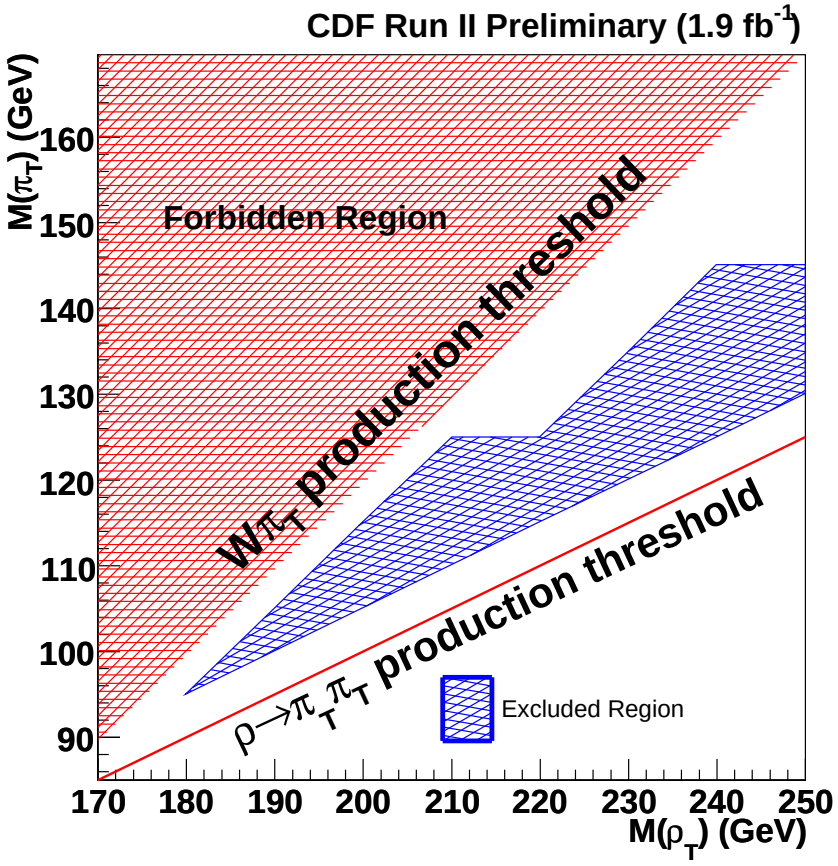

Figure 57: The observed excluded region at 95% C.L. in the ($m(\rho_T)$-$m(\pi_T)$) plane for $\rho_T^{\pm/0} \rightarrow W\pi_T^{0/\mp} \rightarrow l\nu b\bar{q}$ production. The blue region means 95% C.L. observed excluded region. The red region is the forbidden region due to the Wπ_T production kinematical threshold. And the red line is the $\rho_T \rightarrow \pi_T\pi_T$ production threshold.

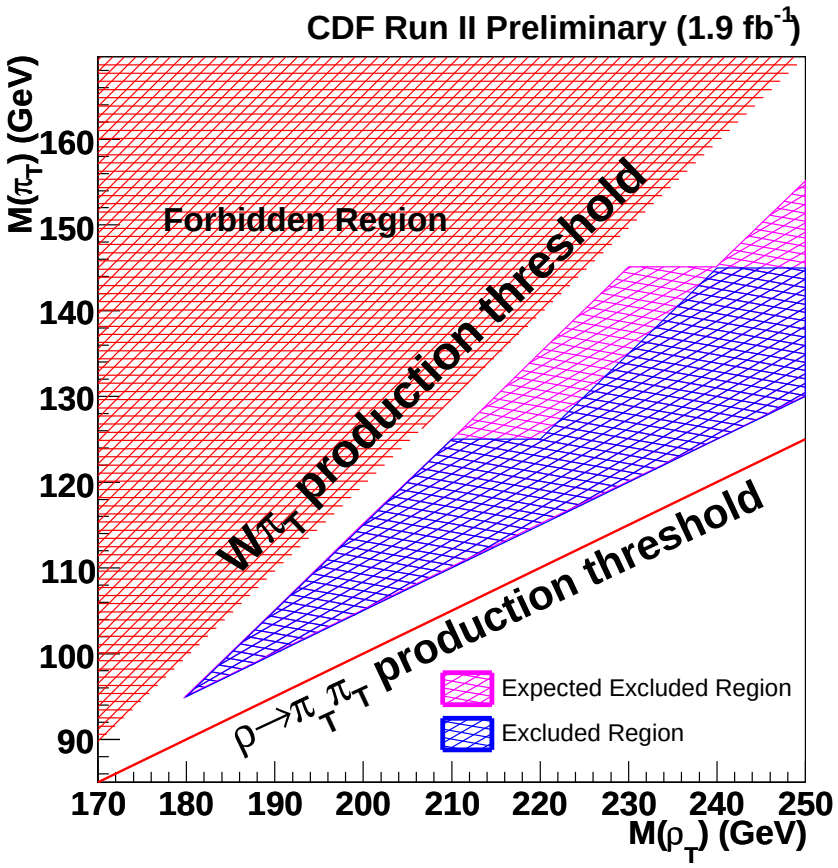

Figure 58: The expected and observed excluded region at 95% C.L. in the ($m(\rho_T)$-$m(\pi_T)$) plane for $\rho_T^{\pm/0} \rightarrow W\pi_T^{0/\mp} \rightarrow l\nu b\bar{q}$ production. The red region is the forbidden region due to the Wπ_T production kinematical threshold. And the red line is the $\rho_T \rightarrow \pi_T\pi_T$ production threshold.

11 Acknowledgments

We would like to thank Kenneth Lane for many useful discussions.

References

[1] Kenneth Lane, "Search for Low-Scale Technicolor at the Tevatron", hep-ph/0605119

[2] T. Masubuchi et al., "Search for Technicolor Particle in Association with $W^{\pm}$ Boson at CDF with $\int \mathcal{L}dt$ = 955 pb^{-1}", CDF Note 8535

[3] T. Masubuchi et al., "Search for Higgs Boson Production in Association with W Boson with 1.7fb-1", CDF Note 8916

[4] T. Masubuchi et al., "Search for the Standard Model Higgs Boson Production in Association with a W$^{\pm}$ Boson using $\int \mathcal{L}dt$ = 1.9 fb^{-1}", CDF Note 9136

[5] H. Bachacou, P.Lujan, M.McFarlane, W.Yao, "Advenced Heavy Flavor Tagging Using a Neutral Network", CDF Note 7742

[6] M. McFarlane et al. "Measurement of ttbar cross section with NN btagging in Lepton + jets events", CDF Note 8188

[7] Franklin, Grinstein, Guimaraes da Costa, Lannon, Schwarz, Sherman and Taffard, "Method 2 Backgrounds for 1.12/fb Lepton+Jets Analysis", CDF Note 8766

[8] D. Amidei et al. "Calibration of Heavy-Flavor Production in W + 1 Jet Data"

[9] Grintein, Guimaraes da Costa, Shrman, "SecVtx Mistag Asymmetry for Winter 2007", CDF Note 8626

[10] Han, Boisvert, "Trigger Efficiencies for the High Et Central Electron in the Gen6 data", CDF Note 8629

[11] Hare, Halkiadakis, Spreitzer, "Electron ID Efficiency and Scale Factors for Winter 2007 Analyses", CDF Note 8614

[12] Grundler, Lovas, Taffard, "High-Pt muons recommended cuts and efficiencies for Winter 2007", CDF Note 8618

[13] S. Grinstein, D. Sherman, "SecVtx Scale Factors and Mistag Matrices for the 2007 Summer Conferences", CDF Note 8910

[14] http://www-cdf.fnal.gov/internal/physics/joint_physics/index.html